THE JOURNAL OF PHYSICAL CHEMISTRY A
A JOURNAL OF THE AMERICAN CHEMICAL SOCIETY

pubs.acs.org/JPCA

Perspective

Molecular Anions Perspective

Jack Simons*

Cite This: https://doi.org/10.1021/acs.jpca.3c01564

Read Online

ACCESS | Metrics & More | Article Recommendations

ABSTRACT: This Perspective attempts to shed light on developments in the theoretical and experimental study of molecular anions highlighting more recent workers in the field. The species I discuss include (i) valence-bound (singly and multiply charged) anions including atmospheric, catalytic, superhalogen, interfacial, and more; (ii) dipole- and correlation-bound anions including their role as doorways to other states and their appearance "in space", and (iii) metastable anions focusing on tools needed for their theoretical treatment. I also briefly discuss angular distributions of photodetached electrons and their growing utilization in experiments and theory. A recurring theme is the dependence of electron binding energies (EBEs) on the surrounding environment. Some anions that are nonexistent as isolated species evolve to be stable but with small EBEs when weakly solvated (e.g., as in a cluster or at an air−solvent interface). Others existing in isolation only as metastable species become stable when the underlying molecular framework contains one or more positively charged group (e.g., protonated side chains in a peptide) that generates a stabilizing Coulomb potential. On the other hand, a destabilizing Coulomb potential between/among negative sites in a multiply charged anion decreases the EBEs of each such site and generates a repulsive Coulomb barrier that can affect stability.

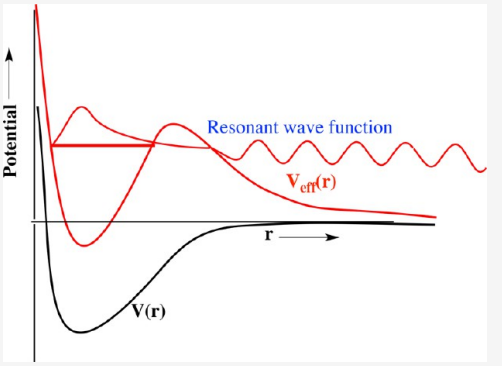

1. INTRODUCTION

In 2008, I published a 110-page article[1] describing the experimental and theoretical study of molecular anions (MAs) highlighting contributions from pioneers of the field. I believe ref 1 remains a good route to gain information about works and earlier workers that have contributed much to this field. Here I highlight work carried out by several new-generation scholars, and I explain why MAs are important to chemistry and how their study often requires special tools (both experimental and theoretical).

To illustrate how chemistry's study of anions has grown in the past ca. 70 years, in Figure 1 I plot the number of articles having "anion" or "anions" in their titles published in all ACS journals dating back to 1940 (the data point labeled 1955 includes work from 1940 to 1955).

There were only 68 papers between 1940 and 1955, but the number grew to 1069 during 2015−2020! I hope these data encourage you to keep reading.

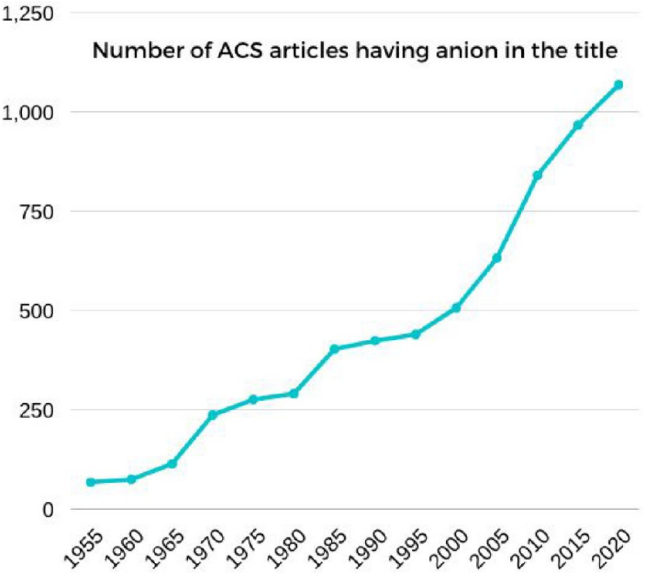

Figure 1. Plot of the number of articles in all ACS journals having anion in the title over five-year intervals.

2. HOW MOLECULAR ANIONS DIFFER FROM NEUTRAL MOLECULES IN IMPORTANT WAYS

Imagine forming a neutral or anion by attaching its last electron to its precursor. In Figure 2, I provide qualitative depictions of the effective potential that this electron would experience as it approaches the corresponding precursor including the constraint[2] that the electron reside in an orbital orthogonal to the other occupied orbital.

Received: March 7, 2023
Revised: April 5, 2023

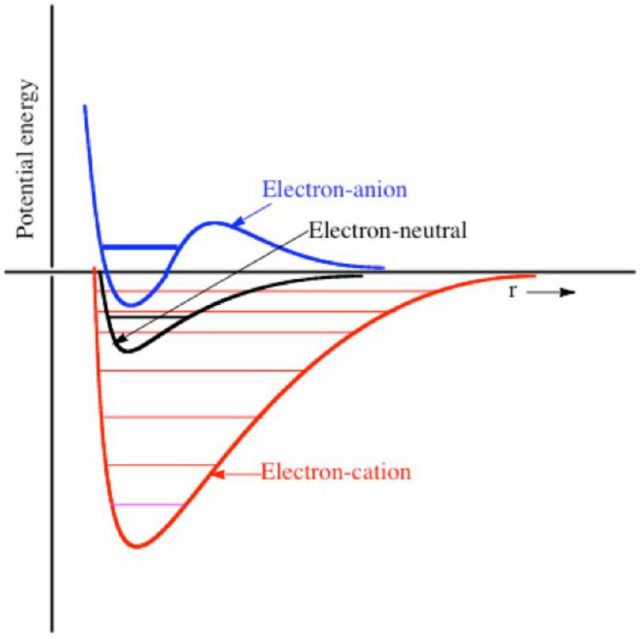

Figure 2. Effective potential as a function of distance r from the electron to the precursor forming a neutral (red), singly charged anion (black), and multiply charged anion (blue). The horizontal lines denote energies of electronic states.

2.A. Neutral Molecules. For a neutral molecule, at large r the potential is attractive and of Coulomb form $-\frac{1}{r}$ (in atomic units where one unit of energy is 27.21 eV). The long-range character of this potential, combined with the fact that valence-range interactions with the precursor cation's electrons come into play at much shorter distances, produces a deep potential well that nearly always supports a large number of bound electronic states, including valence states at low energies and Rydberg states at higher energies extending up to the neutral's ionization threshold. *This multitude of bound states provides a wealth of opportunities for bound-to-bound electronic transitions to be probed by spectroscopy, sometimes with vibrational and even rotational resolution.*

2.B. Singly Charged Anions. For a singly charged anion, there is no attractive long-range Coulomb potential. The potentials operative at large-r are the charge-dipole $-\frac{\boldsymbol{\mu}\bullet\mathbf{r}}{r^3}$, charge-quadrupole $-\frac{\mathbf{Q}\bullet\bullet(3\mathbf{rr}-r^2\mathbf{1})}{3r^5}$, and charge-induced-dipole (often called polarization) $-\frac{\boldsymbol{\alpha}\bullet\bullet\mathbf{rr}}{2r^6}$ potentials. Here $\boldsymbol{\mu}$ is the neutral precursor's dipole moment vector, $\mathbf{Q}$ is its quadrupole tensor, $\boldsymbol{\alpha}$ is the polarizability tensor, $\mathbf{r}$ is the vector position of the electron, and the $\bullet$ symbol denotes contraction of the vector $\mathbf{r}$ with each of the three electrostatic moments.

These potentials vary with distance as r^{-2}, r^{-3}, and r^{-4}, respectively. The absence of the r^{-1} Coulomb attraction causes there to be no Rydberg states; the only bound states are those formed by the combination of valence-range interactions and the long-range dipole, quadrupole, and polarization potentials.

For anions in which the valence-range attractive potential is strong, a bound state can be formed and have a substantial electron binding energy (EBE). HO^-, H_2N^-, H_2C^-, H_3C^-, and $H-COO^-$ are familiar examples with a wide range of EBEs: 1.83, 0.77, 0.65, 0.08, and 3.50 eV, respectively.[3] *However, none of these anions have any valence-bound electronically excited states. In fact, most anions possess at most one valence state sufficiently bound to be experimentally probed.* This is why I show only one horizontal black line in Figure 2. *As a result, valence bound-to-bound electronic spectra are usually unattainable although bound-free spectral probes can still be used, but the amount of information thus derived is much less than in the neutral-molecule case.*

When the valence-range attractive potential is weak, the neutral precursor might not be able to bind the extra electron into any of its valence orbitals, but it is still possible that the long-range dipole, quadrupole, or polarization potential can be strong enough to generate a different kind of bound state.[4] These different bound states are called nonvalence as the electron does not reside in a valence molecular orbital. *It turns out that for most molecules with large $\boldsymbol{\mu}$, $\mathbf{Q}$, or $\boldsymbol{\alpha}$ moments, only a single bound state, if any, occurs with sufficiently large EBE to be experimentally studied.* To illustrate, I show in Figure 3 the orbital into which an electron is bound when attracted to 1,1-dicyanoethylene.

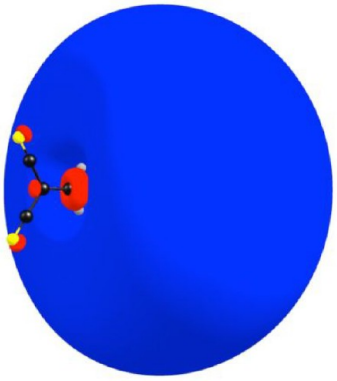

Figure 3. Orbital holding extra electron in 1,1-dicyanoethylene anion. Reprinted with permission from Figure 7 in ref 65. Copyright 2022 American Chemical Society.

This is a case in which the dominant attractive potential is the charge-dipole potential (this molecule has a dipole moment of 5 D) and is illustrative of so-called dipole-bound (DB) anions.[5] Here the EBE is 0.02 eV. In these DB cases as well as when the quadrupole or polarization potentials are dominant, the electron EBEs are very small[6] (often in the 0.001 to 0.1 eV range). This makes it difficult to study them experimentally because (i) one needs to use special techniques to generate such fragile species and (ii) they are susceptible to autodetachment induced by energy transfer from vibrational or rotational degrees of freedom,[7] which can limit their lifetimes.[8]

2.C. Metastable Singly Charged Anions. Some neutral precursor molecules do not form any bound anions at all. They do not have sufficiently strong valence-range attraction potentials or large enough dipole or quadrupole moment or polarizability to capture an extra electron and form a bound state. Nevertheless, some such precursors can still give rise to metastable/temporary anions. These anions can be of much importance in chemical and physical phenomena because, if they live long enough, some of the extra electron's kinetic energy can be transferred to the precursor's vibrational degrees of freedom even to an extent that can break chemical bonds.

Temporary anions can be formed by colliding a free electron with a neutral precursor or by photoexciting from a bound state into the metastable state. *So, what interaction between the precursor and the extra electron gives rise to a state that is metastable?* I will illustrate for so-called shape-resonance states,

https://doi.org/10.1021/acs.jpca.3c01564
J. Phys. Chem. A XXXX, XXX, XXX−XXX

but there are other metastable states of a different character (e.g., states of ethylene anion having $\pi^1\,\pi^{*2}$ character) that I will not be discussing here because they tend to occur at higher energies.

Even though I do not show a long-range repulsion in the black curve of Figure 2 when characterizing the electron-neutral interaction, *if the electron enters a molecular orbital having nonzero angular momentum, there will be a repulsive centrifugal contribution to the potential*. For example, in forming an ethylene anion by adding an electron to its π^* orbital, the electron experiences a long-range repulsion $\frac{l(l+1)}{2r^2}$ whose magnitude results from the (approximate) $l = 2$ character of the π^* orbital shown in Figure 4.

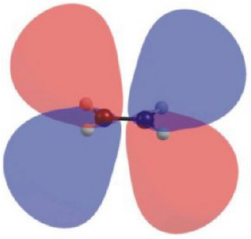

Figure 4. Ethylene's π^* orbital whose symmetry displays $l = 2$ (i.e., *d*-orbital) character. Adapted with permission from Figure 1 in ref 65. Copyright 2022 American Chemical Society.

This centrifugal repulsion causes the net radial electron-molecule interaction to not look like that depicted in black in Figure 2, which I repeat in Figure 5, but like what I show in green in Figure 5.

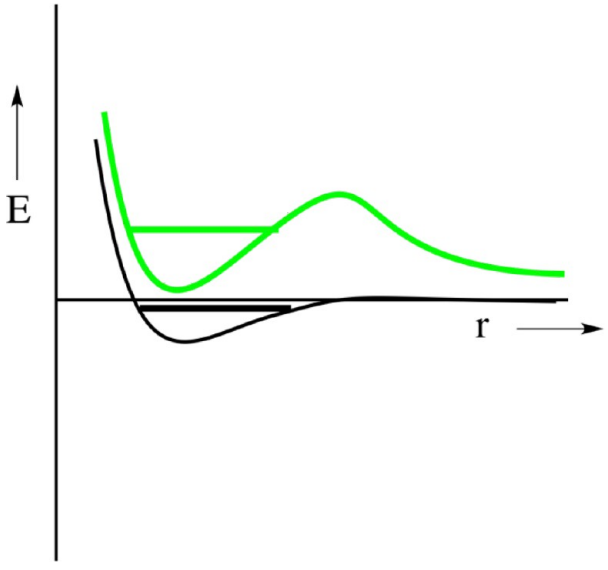

Figure 5. Effective potential for an electron interacting with a neutral precursor in the absence of centrifugal potential (black) and including centrifugal potential (green).

For ethylene, it turns out that the valence-range attractions are not sufficient to render the total potential attractive enough to produce a bound state but they are strong enough to generate a metastable π^*-anion state as I suggest with the green horizontal line in Figure 5. For ethylene, this state lives only a few[9] fs and decays by autodetachment of its excess electron by tunneling through the barrier.

In contrast, for tetracyanoethylene, the valence range attractions are strong enough to make the π^*-attached anion electronically bound (by ca. 2 eV) as its π^* orbital plot in Figure 6 illustrates. So, depending on its substituents, ethylene can be

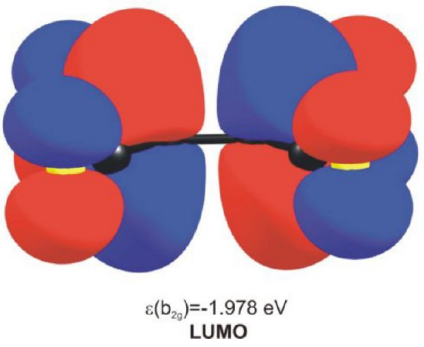

Figure 6. π^*-orbital of tetra-cyano-ethylene. Reprinted with permission from Figure 3 in ref 65. Copyright 2022 American Chemical Society.

involved in strong electron binding (Figure 6), very weak electron binding (Figure 3), or metastable binding (Figure 5).

2.D. Multiply Charged Anions. For a multiply charged anion,[10] the dominant potential at large-r is the repulsive Coulomb interaction $+\frac{q}{r}$ with the underlying negatively charged precursor of charge $-q$. In addition to this repulsive Coulomb barrier[11] (RCB) potential, there can also be a long-range repulsive centrifugal potential $\frac{l(l+1)}{2r^2}$ if the final electron is entering a molecular orbital having nonzero angular momentum l (e.g., $l = 1$ for a p orbital of an atom or for one of the p_π orbitals of the H−N diatomic; $l = 2$ for the π^* orbital of ethylene). For any bound electronic states to arise, the valence-range potentials must be sufficiently attractive to overcome these two repulsions whose magnitude grows even stronger at smaller r.

The Coulomb repulsion exerted on the last electron by the precursor causes many multiply charged anions that we think we are familiar with to have unexpectedly more complicated lives (e.g., O^{2-}, SO_4^{2-}, and PO_4^{3-} do not really exist as isolated bound species although they do when sufficiently solvated). I hint at this issue in Figure 2 where I show the blue potential to not dip sufficiently below the asymptote although I still drew a horizontal blue line suggesting that a metastable state might exist.

In situations where the valence-range attraction does not produce a total potential attractive enough to support a bound state, metastable states can arise, and these can play important roles in chemistry. These states are metastable because they can decay (losing their extra electron) by tunneling through the RCB. So both for multiply charged anions, where the barrier arises from the Coulomb repulsion and (possibly) from centrifugal repulsion, and for singly charged anions having centrifugal repulsion, metastable states can be expected.

I do not want to give the impression that stable multiply charged anions do not exist. Certainly, they do but only when the internal Coulomb repulsions among their charged groups do not exceed the intrinsic electron binding strength of the region(s) in the anion where the last electron is localized. For example, in dicarboxylates $^-OOC-(CH_2)_n-COO^-$ in which the two charges reside largely on the terminal −COO units, the dianion is electronically and geometrically stable if there are more than two methylene units. For $n < 3$, the Coulomb

https://doi.org/10.1021/acs.jpca.3c01564
J. Phys. Chem. A XXXX, XXX, XXX−XXX

repulsion from one $-COO^-$ site exceeds the intrinsic electron binding strength of the other $-COO$ unit, so the dianion is not bound. In addition, longer linear carbon chains such as C_8^{2-} and C_{10}^{2-} support stable dianions, as do species having several ligands among which the excess electrons can be delocalized as in[12] TeF_8^{2-}.

In the presence of stabilizing solvent molecules or counter cations, many of the multiply charged anions that are not stable as isolated species become stable. For example, although SO_4^{2-} and PO_4^{3-} are not stable, $SO_4^{2-}(aq)$ and $PO_4^{3-}(aq)$ are. In fact, many unstable multiply charged anions can be rendered stable by adding just a few solvent molecules.[13] $SO_4^{2-}(H_2O)_n$ is stable for $n > 2$ and $PO_4^{3-}(H_2O)_n$ is for $n > 3$, with both having EBEs that increase as n increases, and $Na^+(SO_4)^{2-}$ is stable[14] and has an EBE of ca. 3.9 eV.

Throughout this Perspective, the effects of solvation, counterions, and repulsive and attractive internal Coulomb potentials[15] will be shown to play key roles in determining stability and EBEs. As illustrated above, repulsive Coulomb potentials reduce EBEs and produce RCBs in multiply charged MAs. As I will discuss later when treating adding an electron to the π orbital of an amide group in a polypeptide containing a protonated side chain, the Coulomb potential generated by the protonated site is attractive and acts in a stabilizing manner.*

3. INTERESTING CLASSES OF MOLECULAR ANIONS, WHERE THEY ARISE IN CHEMISTRY, AND WHY THEY PRESENT SPECIAL CHALLENGES

In this section, I will begin by talking about conventional anions[3] that bind their excess electron(s) in valence orbitals. I should make it clear that when I discuss any specific anion, I am speaking of the anion as an isolated species; if I am discussing an anion that is solvated or surrounded by one or a few "solvent" molecules, I will point this out explicitly.

3.A. Conventional (Valence) Singly and Multiply Charged Anions. When studying a singly charged anion such as HO^-, $H_5C_6O^-$ (phenoxide), or O_2^-, there are two main challenges arising on the theory front. The fact that electron affinities (EAs) are usually considerably smaller than molecular ionization potentials causes the valence electron densities of anions to be more diffuse. This introduces the need to employ extra atomic orbital basis functions (termed diffuse functions) in any electronic structure calculation. This is not a major problem as most widely used quantum chemistry codes allow for the inclusion of such functions, and they are widely available in various basis set libraries. On the other hand, the computational cost when adding these functions to a traditional basis set increases in a manner that scales at least cubically with the number of basis functions.

Another challenge relates to the fact that EAs are usually small fractions of the total electronic energy of the anion (e.g., Cl has a large EA of 3.6 eV; for OH, the EA is 1.8 eV; for CH_3 the EA is 0.08 eV; for dipole-bound anions, the EAs are usually <0.1 eV). This means that the precision of the electronic structure calculation must be very high to allow one to extract (small) EAs by subtracting the (large) total electronic energy of the anion from that of the neutral. This is why EA calculations nearly always involve using high-level quantum chemistry methods that include the effects of electron correlation.

These same theoretical methods can be used as well on multiply charged anions that are electronically stable.

On the experimental front, methods have been invented to overcome what used to be a major difficulty- making the anion. To prepare an isolated stable singly charged anion, a variety of techniques can be used, including the flowing afterglow method introduced long ago. One can use electrospray (ES) of a salt M^+X^- in a solvent S which generates a variety of $X^-(S)_n$ anion clusters and may even generate bare X^-. For a substance X with a reasonable vapor pressure, one can expose X to a flow of gaseous molecules (e.g., Ar or N_2 denoted S) to entrain X molecules and form various neutral $(X)_m(S)_n$ clusters, which can be exposed to a discharge of electrons to subsequently generate $(X)_m(S)_n^-$ cluster anions. As an alternative for species that are not volatile, one can use laser ablation to generate the gaseous X_m clusters. It is also possible to form X^- by deprotonating HX using another anion Y^- having a greater proton affinity than X^-; such reactions are often carried out within an ion-cyclotron resonance (ICR) chamber using a convenient source of Y^- ions. There are other more specialized methods for generating DB anions that I will explain later.

An informative example of a conventional anion's behavior that involves a bound ground state and metastable valence excited states derives from Jan Verlet group's study[16] of doubly deprotonated fluorescein (Fl^{2-}), whose structure is shown[17] in Figure 7. In this dianion the Coulomb repulsion between the

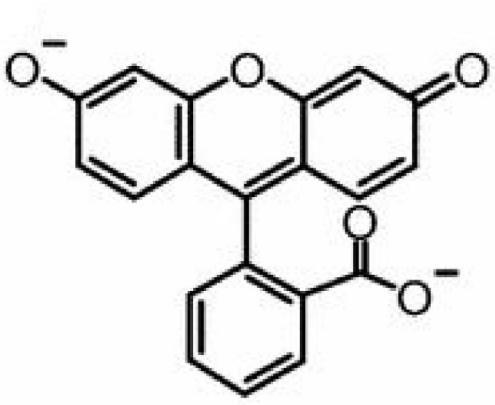

Figure 7. Structure of the doubly deprotonated fluorescein. Reprinted Figure 1 with permission from ref 17. Copyright 2012 American Physical Society.

two negative sites does not overcome the intrinsic EBE of either the carboxylate or the $R-O^-$ group, but it does lower the EBEs of both sites. For example, the authors estimate[16] the EBE of this dianion to be ca. 0.5 eV, which is far below the intrinsic EBE of either site.

This dianion is electronically stable in its singlet ground state (S_0), and in Figure 8a, I show a depiction of the RCB_0 connecting S_0 to the energy of the doublet ground state (D_0) of singly charged Fl^- plus a free electron.

Figure 8a describes the direct detachment of an electron using a photon whose energy exceeds the top of the RCB_0; here the kinetic energies of the electrons ejected into various vibrational levels of Fl^{1-} are show as downward blue arrows. The dianion Fl^{2-} has singlet ππ* excited states S_1 and S_2 that can be accessed by a photon of similar energy to that shown in Figure 8a or with an energy lower than the RCB_1 connecting S_1 to D_0 as suggested in Figure 8b.

If the photon accesses S_1 near its origin, detachment can still occur but the electron must tunnel through RCB_1 as suggested

https://doi.org/10.1021/acs.jpca.3c01564
J. Phys. Chem. A XXXX, XXX, XXX−XXX

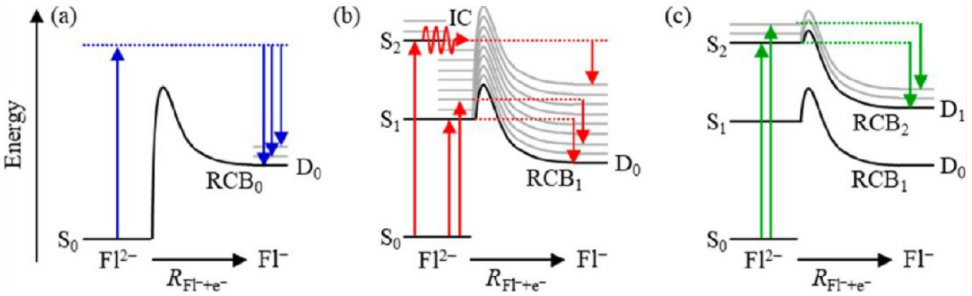

Figure 8. Qualitative plots of the potential energy experienced by the last electron as it approaches the Fl^- precursor anion (a) also showing the RCBs relating to forming the Fl^- in its doublet ground D_0 or excited D_1 state (b) and (c). Reprinted with permission from Figure 3 in ref 16. Copyright 2022 American Chemical Society.

in Figure 8b, so a very small detachment signal is observed in this situation. If S_1 is accessed above the RCB_1 barrier, direct detachment can also be seen; this information allowed the authors of ref 16 to estimate the top of the RCB_0 to be 2.1−2.2 eV above the D_0 state.

If S_2 is accessed, two things can happen. Internal conversion from S_2 to S_1, which Kasha's rule predicts, after which tunneling through RCB_1 to generate D_0 and a free electron can take place as also shown in Figure 8b. Alternatively, detachment from S_2 to the D_1 excited state of the monoanion can take place with or without tunneling through RCB_2, depending on the photon energy as also shown in Figure 8c.

I think this example offers good insight into what one encounters when considering using materials containing multiply charged anions in designing new materials. One needs to understand the nature and lifetimes of the excited states, the presence of RCBs in such states, and how the Coulomb repulsion generated by one negative site on another reduces the EBEs of both.

Another example of how conventional valence-bound anions are impacting chemistry is provided by Caroline Chick Jarrold's work[18] examining anions in atmospheric reactions. In Figure 9 I show a diagram in which a myriad of atmospheric anions appear.

Jarrold has used mass spectral and spectroscopic methods to study many of the anions and reactions listed in Figure 9 with a focus on collision complexes and radical bimolecular reaction complexes. She and Christine Aikens have also done a lot of work studying metal cluster anions[19,20] focusing on their semiconductor and metallic properties, and on using ligands to alter their electronic or magnetic properties.

When it comes to studies of metal clusters, Anastassia Alexandrova's theoretical studies of their anions are important as indicated by her study[21] of bimetallic cluster anions for reducing CO_2 into more valuable chemicals. In Figure 10 I show energy profiles for CO_2 reacting with $PdCuH_4^-$ with the bimetallic cluster existing in either of two geometrical isomers, labeled A and B.

This suggests that formic acid HCOOH is more likely to be formed from the B isomer of the anion, whereas the A isomer's reaction with CO_2 has a significantly higher barrier (red path) to overcome. Such studies illustrate how theoretical simulations can assist in designing optimal species for a desired reaction outcome.

It is not always only spectroscopy and theory that are used to study MAs. In Caroline Dessent's lab,[22] photo dissociation and mass spectrometry were used to study the competition between fragmentation and electron detachment involving MAs consisting of the deprotonated forms of two molecules used in

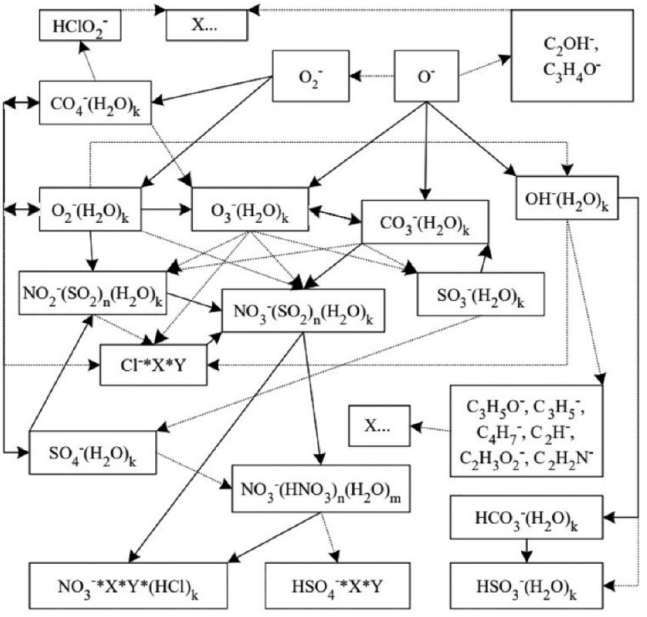

Figure 9. Illustration of how O_2^- is involved in forming or reacting with many other atmospheric species and generates other anion. Adapted from Figure 1 in ref 18 with permission of the American Chemical Society.

sunscreens. Such an approach was important in determining how long these molecules could protect against UV radiation before being photodegraded.

There exists a family called superhalogen anions[23] pioneered by Boldyrev and Gutsev that have EBEs exceeding those of halogen anions. These anions are often formed from one or more central metal atom M in a high oxidation state surrounded by several negatively charged halogen or pseudohalogen (e.g., CN^-, OCN^-, etc.) ligands. They have been suggested to be good candidates, for example, as counterions in Li-ion batteries and in ionic liquids. Piotr Skurski[24] and Iwona Anusiewicz's[25] groups have been especially active recently in advancing this field, and refs 24 and 25 provided excellent overviews.

Another recently studied family of MAs is called solvated-electron precursor (SEP) anions where the Ortiz and Miliordos groups[26,27] have been pioneers. These anions consist of a cation of an electropositive atom M surrounded by neutral closed-shell solvent ligands L and with "extra" electrons attached to the cluster's periphery. $Be^{2+}(NH_3)_4$ with three peripheral electrons attached to form $Be(NH_3)_4^-$ is an example studied[26] early in these authors' work. They have extended their studies[27] to systems with two solvent shells including cores consisting of

https://doi.org/10.1021/acs.jpca.3c01564
J. Phys. Chem. A XXXX, XXX, XXX−XXX

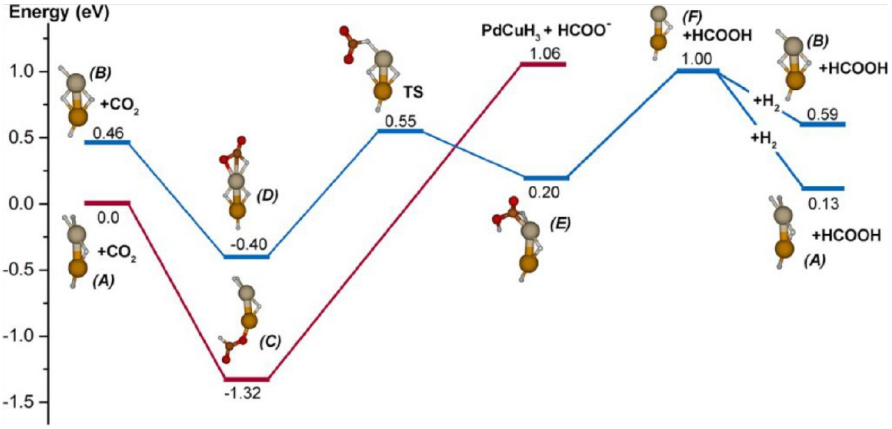

Figure 10. Reaction paths for converting CO_2 into formic acid. Adapted with permission from Figure 4 in ref 21. Copyright 2020 American Chemical Society.

$M(NH_3)_4@12NH_3$ with M = Li, Be^+, and B^{2+}, and they have done so for cases in which fewer peripheral electrons are attached to form either neutral or positively charged species. In addition, they have made interesting observations about the aufbau-principle that applies to these species orbitals. The SEP anions are somewhat derivative of the class of double-Rydberg anions such as NH_4^- that Ortiz studied[28,29] after being discovered experimentally[30] by Bowen.

In closing this discussion of valence-bound anions, I want to mention one more aspect of how solvation (full or partial) influences the behavior of MAs. *It is thought that anions tend to congregate toward air−water interfaces*[31] *because their large sizes (related to the diffuse nature of their outermost orbitals) cause their presence to substantially disrupt water's hydrogen bonding network.* This is illustrated in Figure 11 where the radial distributions of cations (H^+ and Na^+) and anions (Cl^-, Br^-, and OH^-) near a computer-simulated air−water interface are shown.

Although the degree to which these anions congregate near the interface differs from anion to anion (Br^- being most prone), it is clear that the concentration of ions near such surfaces is likely to substantially exceed the bulk concentration. Keeping in mind what I said earlier[13] about how SO_4^{2-} has a much lower EBE when surrounded by only a few H_2O molecules than in bulk solvation conditions, *one should therefore expect the behavior of anions at air−water, ice−water, and other interfaces to be considerably different from their behavior in bulk.* This is especially important to be aware of in atmospheric and nanoscience studies where the surface area to volume ratios of the species studied can be quite substantial.

To further illustrate this point, I note that the Zare group recently reported[32] finding that H_2O_2 is generated from sprayed 1−20 μm droplets of pure water. These workers found the H_2O_2 yield to be highest for the smallest droplets, suggesting the process takes place at the droplet's surface. They proposed that, near the surface, the OH^- ions generated from H_2O are sufficiently influenced by the strong local electric field[33] to permit OH^- to lose the excess electron to generate OH radicals which go on to generate the H_2O_2. Their proposed mechanism is shown in Figure 12.

Two key points in this example are (i) that dissociation equilibria might not be the same at surfaces as in bulk[34] and (ii) that local fields[33] at surfaces might facilitate electron detachment.

It turns out that in a recent collaboration Kit Bowen's group has noticed[35] that sprayed water microdroplets containing CO_2

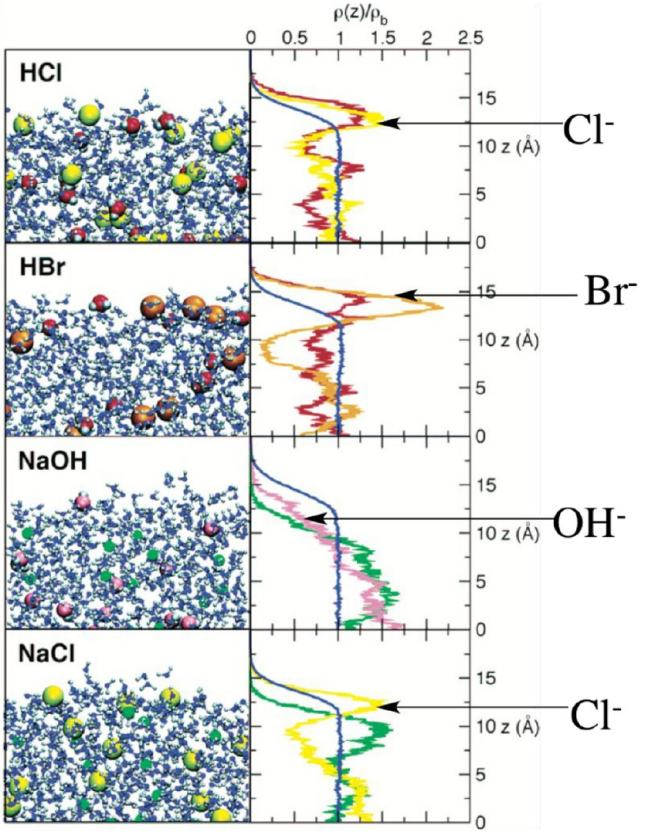

Figure 11. Snapshot of simulation of 1.2 M solutions (left); ions' spatial distributions near air−water interface (z = 15 Å) into the bulk (z = 0) with OH^- oxygen shown as pink; Cl^- as yellow, Br^- as orange. Adapted with permission from Figure 1 in ref 31. Copyright 2005 American Chemical Society.

$$2H_2O \leftrightarrow H_3O^+ + OH^-;\ \text{pH may not be 7.0}$$

$$OH^- \rightarrow e^-(solv.) + HO\bullet;\ \text{helped by strong E field}$$

$$2HO\bullet \rightarrow H_2O_2$$

Figure 12. Summary of the mechanism suggested in ref 32.

and $I-C_6F_5$ can cleave the I−C σ bond to produce $C_6F_5^-$, which subsequently reacts with CO_2 to generate $F_5C_5CO_2^-$ which they then detect. These authors suggest that free electrons are

https://doi.org/10.1021/acs.jpca.3c01564
J. Phys. Chem. A XXXX, XXX, XXX−XXX

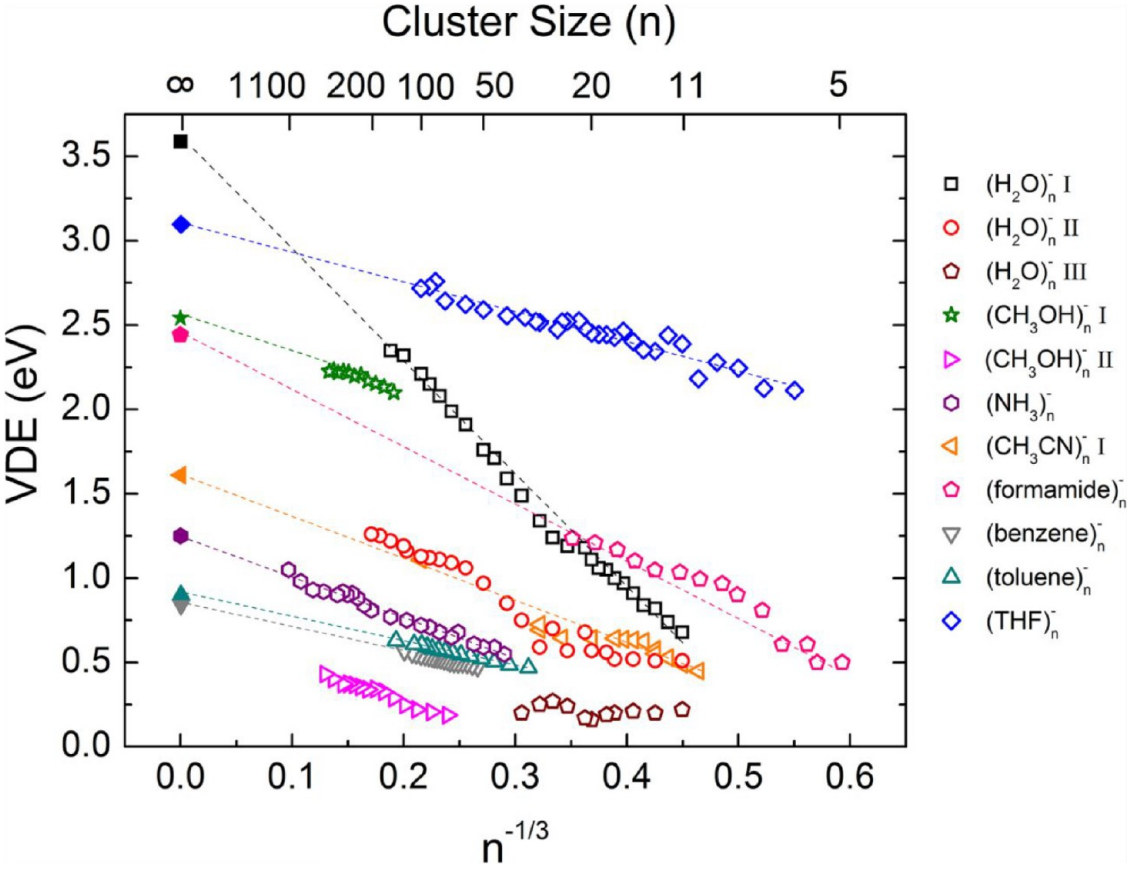

Figure 13. Electron binding energies of several families of M_n^- cluster anions. Reprinted with permission from Figure 4 in ref 42. Copyright 2012 American Chemical Society. The notation I, II, and III labels clusters of different geometric structure.

generated in the sprayed water droplets in higher than expected (in bulk) concentrations, much like Zare proposed in ref 32.

3.B. Dipole-Bound Anions and Similar Species. In Figure 3, I showed an example of the orbital into which an extra electron is attached to form a DB anion. These ions might appear to be exotic, and one might doubt the extent to which they impact chemical science, but I hope to show you that they are important. First, I want to make brief comments on some of the experimental and theoretical challenges[1,5,6] they present.

DB anions occur in a variety of environments, but to create one in isolation is not easy. If the precursor X has a reasonable vapor pressure, one can entrain it in a flow of gaseous S to generate X_nS_m clusters and subject these clusters to low-energy electrons as was discussed earlier. However, this route is likely to succeed only if the resultant clusters have EBEs of 0.1 eV or higher. For example, bathing a gaseous sample of the neutral $(H_2O)_nAr_m$ cluster precursor in low-energy electrons can be used to form $(H_2O)_nAr_m^-$ anions, as the Johnson group has often done.[36] A different pathway is used to form DB anions of very low electron binding strength involves allowing the precursor molecules to collide with atoms that have been excited into a Rydberg state. By tuning the laser to populate Rydberg levels lying δE below the A atom's IP, with δE chosen to match the EA of the DB state, collisions between the precursor and the excited atom can generate the DB anion through a resonant-energy electron-transfer process. By monitoring the abundance of negative ions of the proper mass as the laser's energy is tuned to δE, one can determine the EA of the DB anion. This approach has been used, for example, by Bowen's group.[37]

In some cases, one has a molecule that forms a valence-bound anion and has a large enough dipole moment to form a DB excited state; H_2CCN^- is such an anion. In these situations one can form the valence-bound (VB) anion using, for example, ES or deprotonation and then tune a laser to populate the DB state by excitation from the VB state.

When it comes to the theoretical study of DB anions, two challenges are faced. First, one must use atomic orbital basis functions that are sufficiently diffuse to describe the spatial extent of the DB orbital. As Figure 3 demonstrates, these orbitals' radial extent can be much larger than for conventional valence orbitals. The diffuse basis functions included in most quantum chemistry basis set libraries are not sufficient, but specialized bases[38] have been designed and made widely available. The second challenge that DB states present has to do with electron correlation.[39] Although the electron bound within the DB orbital resides to a large extent far away from the precursor's valence electrons, it still has a significantly large dispersion-like interaction with the latter electrons to contribute substantially to the EBE. That is, the DB orbital is quite polarizable, so it would be expected to have a substantial van der Waals (i.e., dispersion) interaction with other nearby electron densities. It has been shown that including electron correlation effects in electronic structure calculations of DB anions is important.

Now, I want to give you an idea of where DB anions occur and are of importance in chemistry. *In recent years, astro-chemists have concluded that DB anions such as* $C_{2n+1}N^-$ *and* $C_{2n}H^-$ *appear in interstellar space*, with abundances influenced by the dipole moment of the radical precursor. For example, C_6H^- is more

https://doi.org/10.1021/acs.jpca.3c01564
J. Phys. Chem. A XXXX, XXX, XXX−XXX

abundant than C_4H^- although neutral C_4H (μ < 2 D with a $^2\Sigma$ ground state) is more abundant than C_6H (μ > 2 D with a $^2\Pi$ ground state). Because the DB orbital is so diffuse and localized primarily outside the precursor's valence framework, DB anions tend to have geometries very close to that of their precursor. The radio-wave rotational spectrum of DB anions is thus very similar to that of the neutral; this and the fact that linear species have more simple rotational spectra has made the identification of linear interstellar DB anions more possible. In Ryan Fortenberry's excellent review[40] focusing on how electronic structure theory can help in searching for and proposing new potential interstellar anions and Millar's very detailed review[41] of ions in space, you will find much more about this.

Earlier, I mentioned water cluster anions $(H_2O)_n^-$ and said they could be viewed as DB species. Most of the smaller members have stable structures in which the excess electron is bound on the cluster's surface rather than in the interior. As such, they can be viewed as DB anions with the dipole potential involving several if not all the water molecules in the cluster, and they can have EBEs in the tenths of an eV range, which is rather large for DB species. In Figure 13, I show data from a review article[42] from the Neumark lab illustrating how the EBE varies with the number of molecules involved for various isomers of water cluster anions as well as cluster anions comprised of other molecules. The EBEs are plotted as functions of $n^{-1/3}$, which, for a spherical cluster would be inversely proportional to its radius.

In Figure 14 I show the structure, DB orbital, and photodetachment spectrum[36] of one such cluster $(H_2O)_7^-$

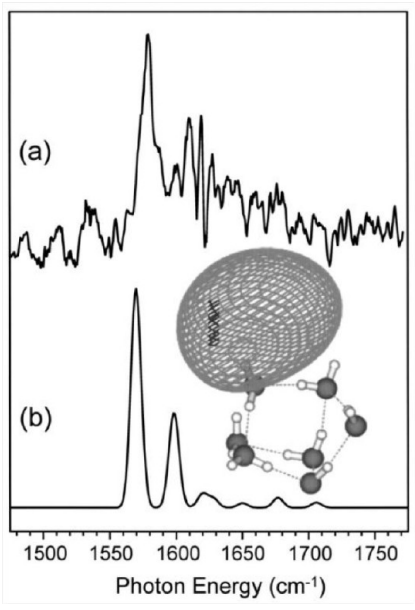

Figure 14. Experimental (a) and calculated (b) photodetachment spectrum of $(H_2O)_7^-$ with the computed minimum-energy structure and DB orbital also shown. Adapted with permission from Figure 8 in ref 36. Copyright 2008 AIP Publishing.

which has an EBE near 0.2 eV. In this structure, you can see how the DB orbital is positioned relative to the nearest H_2O molecule that has both of its O−H bonds directed outward toward the orbital. This motif is characteristic of this class of DB species; that is, even in larger clusters, one of the surface H_2O molecules is oriented in this way and the DB electron is closest to this water molecule. Because $(H_2O)_7^-$ has an EBE of 0.2 eV, infrared excitation is sufficient to detach an electron which has allowed, in particular, Mark Johnson's group[36] to utilize IR spectral methods on these ions.

Another variant of DB anions involving water molecules occurs when an electron initially bound to a solvated conventional anion (e.g., $I^-(aq)$) is photodetached as illustrated in Figure 15. The ejected electron can (a) be fully ejected from the solution (especially if the I^- is near the surface), (b) be captured by nearby solvent molecules which have undergone reorientation to form a solvation cage around the electron, or (c) be captured by nearby solvent molecules whose instantaneous dipole orientations happen to be favorable to forming a DB state. The latter two cases arise is so-called charge-transfer-to-solvent (CTTS) electronic transitions.[43]

In the study of how low-energy electrons induce bond cleavage in biological molecules, DB states have also been suggested to play a role.[44] For example, DNA's nucleobases have dipole moments large enough (2.5−6.5 D) to support DB anion states. It has been suggested that free electrons created by ionization of water molecules or of proteins might initially attach to a base DB orbital and subsequently undergo a DB-to-π^* or -σ^* transition into a base π^* or σ^* orbital as an early step in the bond-cleavage process. *In this context, the DB state is said to be a doorway to the bond-breaking.*

In Figure 16, I illustrate this concept from a computational study[45] of electron attachment to the RNA base uracil (U).

On the left, you see the energies of the DB U^-, of neutral U, and of the state in which the excess electron resides in a N−H σ^* orbital, plotted as functions of the N−H bond length. Also shown is the avoided crossing between the DB and σ^*-attached states that gives rise to a barrier to be surmounted for bond cleavage to occur. On the right, the N−H σ^* orbital is shown.

The Kim group[46] has also interpreted their experimental results on *o*-, *m*-, and *p*-iodophenoxide in terms of a DB doorway state. These anions have valence-bound closed-shell ground states as well as DB excited states. Photoexcitation into the DB states is suggested to then allow for a transition into a repulsive C−I σ^* orbital which leads to C−I bond rupture. Kim's group has published a very significant number of new experimental findings on such MAs and processes.

An analogous mechanism for cleavage of base-sugar N−C bonds in isolated DNA nucleosides and nucleotides, has also been suggested.[45] This may indeed be what happens in the gas phase, but I think this DB doorway mechanism is less likely to be involved in condensed-phase DNA damage[47] where "crowding" might preclude formation of the DB species. When it comes to DNA within cells or even when surrounded by many solvent molecules, I think another mechanism is likely to be operative because the DB state is unlikely to exist in such a crowded environment. In Figure 17 I illustrate this alternative mechanism[48] applied to the cytosine-based nucleotide.

In this proposed mechanism, a low-energy electron strikes one of DNA's bases initially generating an anion in which the extra electron is captured by a base π^* orbital. This orbital is shown in the center of Figure 17. Then, if either the base-sugar N_1−C bond or the more distant sugar−phosphate C−O bond becomes sufficiently elongated (i.e., by vibrational motion), the energy of the π^*-attached state can be crossed by that of the N−C or C−O σ^*-attached state as suggested on the left in Figure 17. In a theoretical study,[48] it was shown that the crossing point for C−O bond cleavage occurred at a lower energy along such a dissociation path primarily because of the very high EA of the phosphate groups. The migration of the attached electron from

https://doi.org/10.1021/acs.jpca.3c01564
J. Phys. Chem. A XXXX, XXX, XXX−XXX

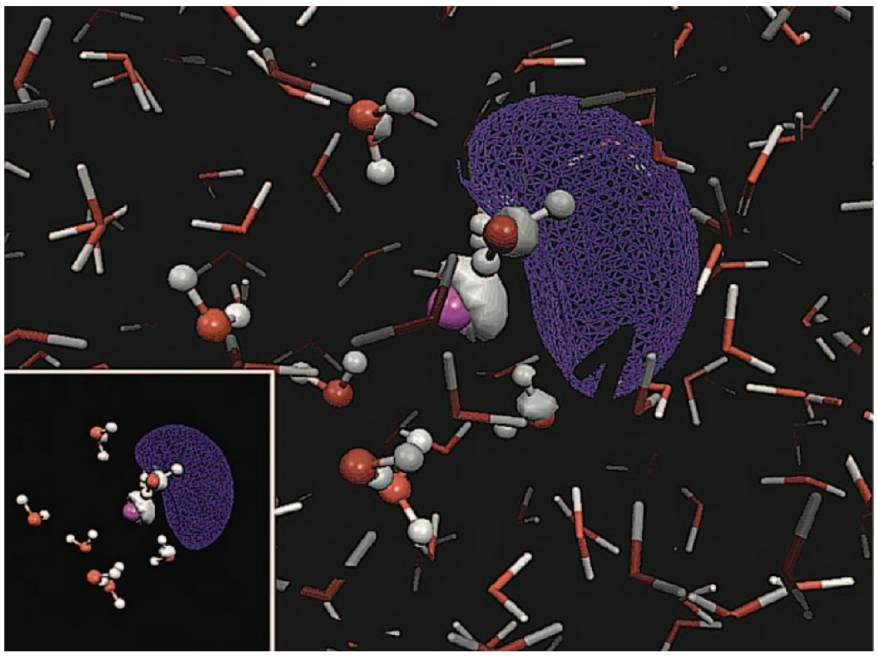

Figure 15. Examples of electron captured on the surface (bottom left) or in a CTTS process (upper right). Adapted with permission from Figure 6.7 in ref 1. Copyright 2008 American Chemical Society.

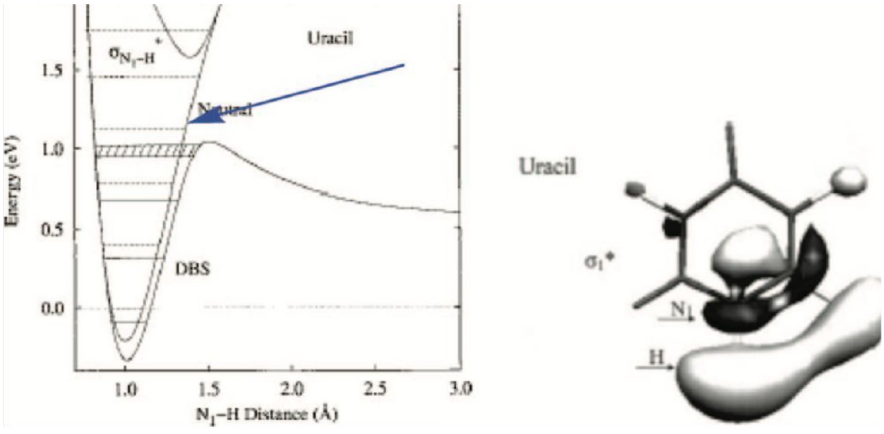

Figure 16. Illustration of doorway process involving DB orbital coupled to N−H σ^* orbital of uracil. Adapted with permission from Figures 3 and 5 in ref 45. Copyright 2006 AIP Publishing.

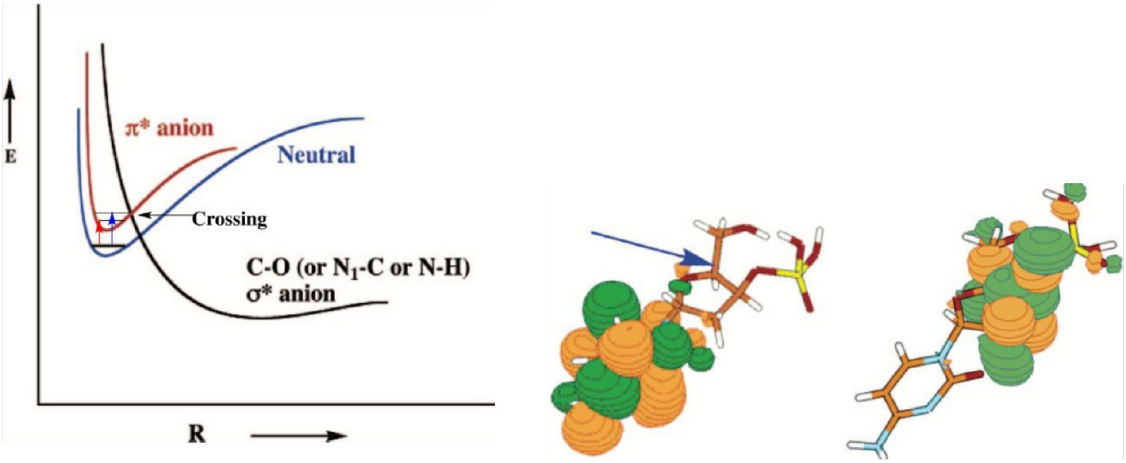

Figure 17. Description of sugar−phosphate C−O bond cleavage caused by electron attachment to base π^* orbital. Adapted with permission from Figure 8 in ref 48. Copyright 2006 American Chemical Society.

https://doi.org/10.1021/acs.jpca.3c01564
J. Phys. Chem. A XXXX, XXX, XXX−XXX

the π^* orbital (center of Figure 17) into the sugar−phosphate C−O σ^* orbital is shown on the right in Figure 17. Subsequent experiments[49,50] showed that this kind of bond rupture occurred and at electron kinetic energies consistent with entering a DNA base π^* orbital.

I should note that in the mechanism just described the π^*-attached state would be metastable for an isolated nucleotide, although it is possible that in solution or a cellular environment, it could be rendered stable by solvation. As shown in Figure 17, the σ^*-attached state would also be metastable to the left of its crossing with the neutral state. I mention this because the study of such a mechanism required using one of the techniques for studying metastable states, which I discuss in subsection 3.D. Recently, a very nice paper appeared[51] in which the authors studied the uracil anion with varying numbers of water molecules attached $U^-(H_2O)_n$. They studied electron detachment induced by exciting from the ground doublet state D_0 of the anion into excited states belonging to the π_2^* and π_3^* states of the uracil anion as well as direct detachment into the singlet ground state of the neutral $U(H_2O)_n$. Using the vertical and adiabatic detachment energies of $U^-(H_2O)_n$ to extract a Marcus-theory reorganization energy, they were then able to extrapolate the ground $U^-(H_2O)_n$ to (i) ground $U(H_2O)_n$, (ii) π_2^* $U^-(H_2O)_n$, and (iii) π_3^* $U^-(H_2O)_n$ energy gaps from $2 < n < 35$, where they had data, to the bulk ($n \rightarrow \infty$). Their conclusion is that both the π_2^* and π_3^* states of the anion can be rendered stable in solution and provide a route by which capture of free electrons can generate the ground-state $U^-(H_2O)_n$ anions.

Finally, I want to show an example of an anion that is very weakly bound but is not of the DB class; instead its electron binding results largely from the large polarizability of the C_6F_6 precursor. This neutral molecule has a planar equilibrium geometry in which it can bind an electron by ca. 0.4 eV using a diffuse orbital analogous to DB orbitals.

In the experiments,[52−54] an I^- anion was complexed with C_6F_6 as shown in Figure 18.

A 3.10 eV pump laser was then used to effect an electron transfer from the I^- ion to the (planar) C_6F_6. A 1.55 eV probe laser was fired at a time τ later, and the photodetached electrons were detected and their kinetic energies (KEs) recorded. It was found that at very short τ, the detached electrons' KEs peaked near 1.1 eV (suggesting the nascent planar $C_6F_6^-$ to have an EBE of 0.45 eV). At $\tau \approx 100$ fs, the KEs of the ejected electrons peaked at a much lower kinetic energy indicating that the electron was now more strongly bound. These workers suggested that at the later time, the $C_6F_6^-$ anion had undergone a "buckling" distortion to move toward its nonplanar equilibrium geometry shown in Figure 19 where the electron resides in a valence-type orbital. In Figure 19, I show the orbitals occupied in the correlation-bound planar geometry and the buckled valence anion's equilibrium geometry as found[55] by the Jordan group.

3.C. Angular Distributions: A Side Adventure. Before moving on to discuss metastable anions, I want to say a bit about how the measurements and theoretical treatments of angular distributions of MAs' ejected electrons have blossomed in recent years. Briefly, when an electron is ejected from an orbital of spherical s symmetry in an electric-dipole transition, the electrons are ejected in a p-wave distribution as suggested[56] in the top row of Figure 20.

Ejection of an electron from an orbital of p symmetry generates an electron wave consisting of a mixture of s and d symmetries as also shown in Figure 20. When an electron is

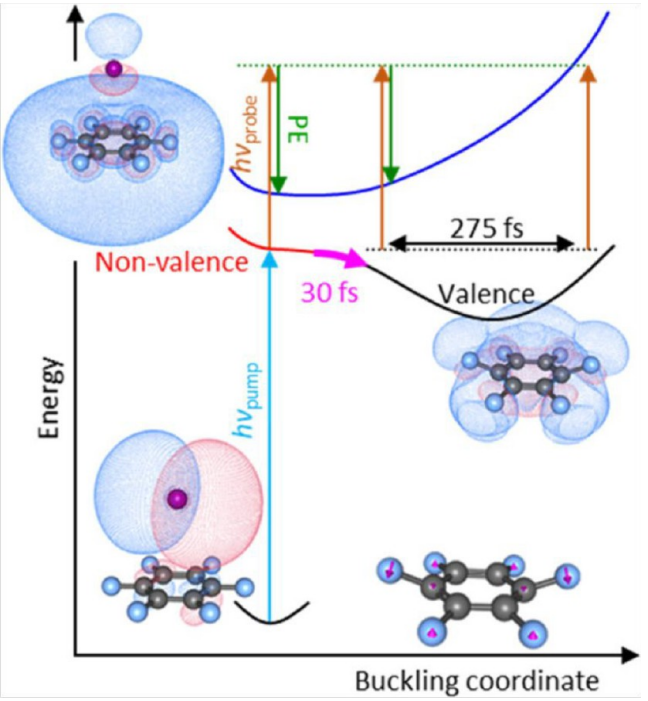

Figure 18. Illustration of photoinduced electron transfer from I^- to planar C_6F_6 followed by relaxation to nonplanar geometry. Reprinted with permission from Figure 8 in ref 54. Copyright 2020 American Chemical Society.

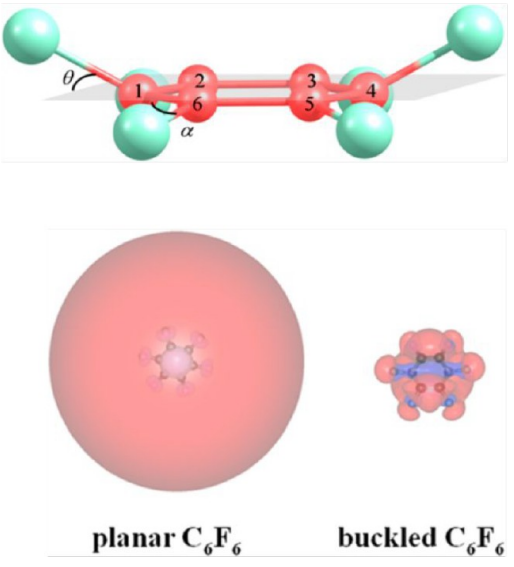

Figure 19. Polarization-formed orbital of planar $C_6F_6^-$ anion and valence orbital of nonplanar anion. Adapted with permission from Figure 16 in ref 7. Copyright 2020 American Chemical Society.

detached from an orbital of mixed s and p character $\Psi = \sqrt{f}\mathrm{p} + \sqrt{1-f}\mathrm{s}$, the angular distribution[57,7,58] results from a combination of the two components as well as interference between them.

It is convention to express the intensity $I(\theta)$ of electrons ejected at angle θ relative to the polarization vector of the detaching photon as

$$I(\theta) \propto [1 + \beta P_2(\cos\theta)] \quad (1)$$

where

https://doi.org/10.1021/acs.jpca.3c01564
J. Phys. Chem. A XXXX, XXX, XXX−XXX

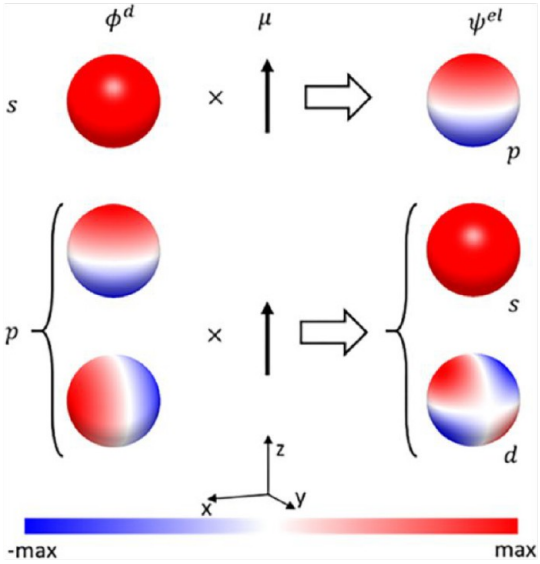

Figure 20. Angular distributions of electrons ejected from s- or p-symmetry orbitals. Adapted with permission from Figure 1 in ref 56. Copyright 2021 American Chemical Society.

$$P_2(\cos\theta) = \frac{1}{2}[3\cos^2\theta - 1] \tag{2}$$

and to use $I(\theta)$ data fit to this functional form to determine a value for the β parameter. This parameter depends on the s/p mixing parameter f and on the dipole-transition probabilities for *s-to-p*, *p-to-s*, and *p-to-d* transitions. β also depends on the KE of the ejected electron, which, in turn depends on the photon's energy.

It turns out that β can be expressed as

$$\beta = \frac{2Z^*(A^*\mathrm{KE}) + 2(A^*\mathrm{KE})^2 - 4(A^*\mathrm{KE})\ \cos(\delta_2 - \delta_0)}{1 + 2(A^*\mathrm{KE})^2 + Z^*(A^*\mathrm{KE})} \tag{3}$$

A^*KE involves the kinetic energy KE and a factor A proportional to the ratio of the p → d and p → s dipole matrix elements, while the Z parameter is defined as

$$Z = \frac{B}{A} * \frac{1-f}{f} \tag{4}$$

The s/p mixture factor f enters in Z as does a parameter B involving the ratio of the s → p and p → s matrix elements. The term $-4(A^*\mathrm{KE})\cos(\delta_2 - \delta_0)$ in the numerator of eq 3 arises from the interference of the s and d components ejected from the p portion of the orbital. The dependence of this complicated expression on A^*KE and on the f parameter is illustrated in Figure 21 where ε is used to denote KE.

For detachment from a nearly pure *s* orbital, $f \approx 0$, and the β value should change rapidly from zero near threshold (KE = 0) and approach 2.0 as KE increases. In detachment from a purely *p* orbital, $f \approx 1.0$, the β value should be near zero at low KE, become negative as KE increases, and evolve into positive values at high KE.

This example shows how measuring the angular distribution, especially if it can be done for a range of KE values, can be a valuable tool for determining the nature of the orbital from which the electron is detached. In this discussion of angular distributions, it is important to point out the major contributions that Richard Mabbs has made on the experimental front and, by collaborating

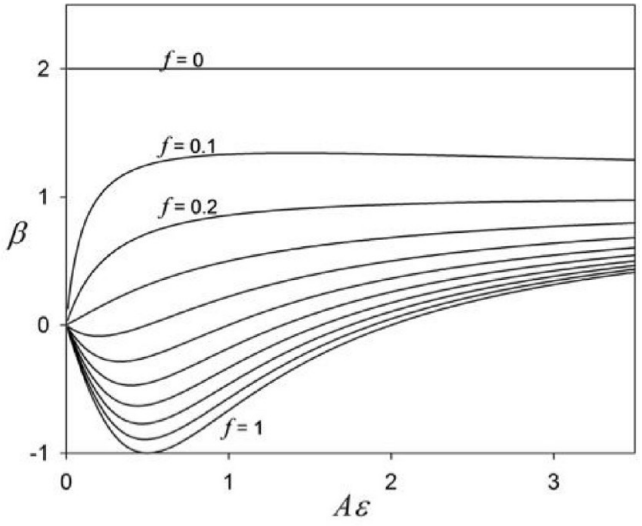

Figure 21. Dependence of β on electron kinetic energy for orbitals of mixed s/p symmetry. Reprinted with permission from Figure 2 in ref 7, Copyright 2020 American Chemical Society.

with Anna Krylov, bringing angular distributions into the mainstream of quantum chemistry calculations. Mabbs and Andrei Sanov[57,58] have used angular distribution for many years to interpret their experimental data and have been among the primary recent chemistry pioneers to this field.

In a collaboration,[56] Mabbs and Krylov examined detachment from the, $^1\Sigma \rightarrow {}^2\Sigma$. transition in CN^-, where the electron is ejected from an orbital of mixed s/p character. The experimental angular distribution produced β values were found to vary with KE as shown in Figure 22a.

When using EOM-IP-CCSD theory, employing the resultant Dyson orbital[59,60] to describe the orbital from which the electron is detached and using a plane-wave function[61] for the outgoing electron, the β-vs-KE curve shown as a dashed line in Figure 22b was obtained (the experimental data is duplicated in gray). Clearly, the theoretical treatment did not yield quantitative agreement. Referring back to Figure 21, the calculated β-vs-KE curve suggested that the orbital from which detachment took place was nearly pure s in character.

This collaboration team then explored whether improving the description of the outgoing electron's orbital to move beyond the plane-wave treatment and incorporating the effect of the CN molecule's dipole moment would help. By carrying out calculations using an out-going electron orbital designed to experience a dipole moment D, they obtained the series of β-vs-KE data shown in Figure 22c. These results suggest a value near D = 0.3 au (ca. 0.76 D) can fit the experimental data, and, importantly, they suggest that theory needs to move beyond a plane-wave treatment for the ejected electron.

In another collaboration,[62] Mabbs teamed up with Krylov and Thomas Jagau to interpret the spectra obtained when the bound $^2\Sigma^+$ ground states of CuF^- and AgF^- are excited to metastable $^2\Sigma^+$ and $^2\Pi$ excited states. Not surprisingly, the angular distribution data obtained in that study allowed the authors to determine the characters of the orbitals from which the electron was ejected. However, it also allowed them to probe how various vibrational levels within these metastable states induced vibration-to-electron ejection. I think these examples illustrate why angular distributions are likely to become even more widely used in experimental and theoretical studies of MAs.

https://doi.org/10.1021/acs.jpca.3c01564
J. Phys. Chem. A XXXX, XXX, XXX−XXX

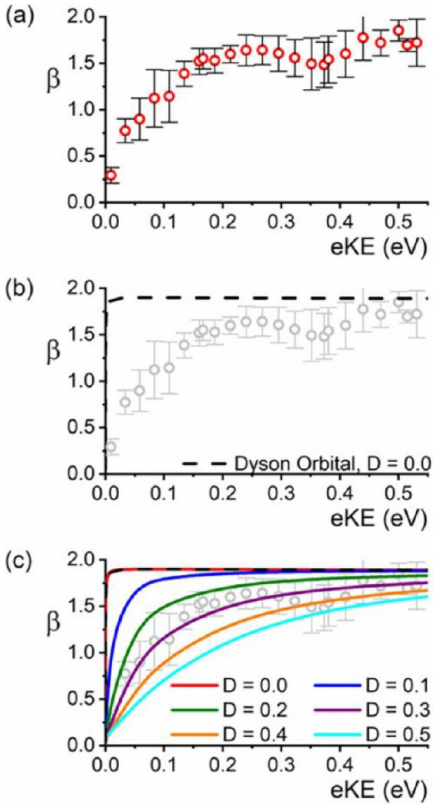

Figure 22. KE-dependence of β from experiment (a) and from modified theory (c) assuming a range of dipole moments D (in atomic units). See text for detail on (b). Reprinted with permission from Figure 2 in ref 56. Copyright 2021 American Chemical Society.

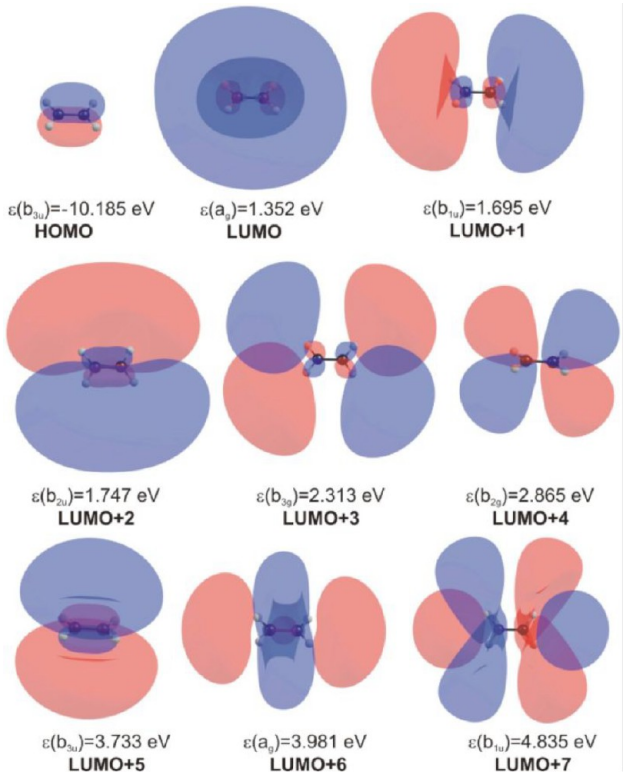

Figure 23. HOMO and several virtual orbitals of ethylene. Reprinted with permission from Figure 1 in ref 65. Copyright 2022 American Chemical Society.

3.D. Metastable Anions. To illustrate the theoretical challenges in studying metastable anions,[1,6,63,64] let me begin by considering what happens if one tries to use a conventional (Koopmans' theorem (KT) from Hartree−Fock in this example) ab initio method to study the π^*-attached state of the ethylene anion. In Figure 23, I show plots of the occupied π of ethylene[65] along with the eight lowest-energy virtual orbitals along with their KT orbital energies.

Because of ethylene's high degree of symmetry, it is easy to "guess" that LUMO+4 might be the π^* orbital and that its energy might offer a good estimate of the energy of the metastable π^*-attached state relative to that of neutral ethylene. The other virtual orbitals shown are pseudocontinuum (PC) orbitals offering qualitative descriptions of a neutral ethylene molecule plus a free electron whose kinetic energy is given by the KT orbital energy. However, this interpretation of LUMO+4 is not entirely correct because if one were to perform the same kind of calculation using different basis sets, one would find that the orbital energies of the lower virtual orbitals would be different, the one that looks like the π^* orbital might not be LUMO+4, and the energy of the orbital that looks to be π^* would depend on which basis was used. This is because the actual π^* orbital resides within and is coupled to the continuum of the ethylene-plus-free-electron system and different basis sets (or different electronic structure methods) will approximate the π^* orbital differently. So, how do you find the correct description of the π^* orbital?

The two most widely used tools for addressing this task are stabilization and complex absorbing potential[66−68] (CAP) methods, both of which I will now briefly explain. The stabilization method[69−71,68] has two variants: one aimed mainly at determining the energy of the metastable state, and another that gives the energy and lifetime.

An easy-to-use method of the first kind[72,69] involves adding to the one-electron component of the Hamiltonian terms that differentially stabilize valence-range orbitals compared to the PC orbitals. In the ethylene example, one could add[65] to the two C nuclear charges and amount δq and add to the four H nuclear charges a counterbalancing $-\delta q/2$. One then carries out a series of calculations with various δq values and plots the virtual orbitals' energies as shown in Figure 24.

Such a plot allows one to move the energy of the more valence-like π^* orbital into the bound-state range for $\delta q > 1.75$ while having less effect on the energies of the PC virtual orbitals which have more of their amplitudes farther from the partial charges. Once $\delta q > 1.75$ and the anion state is bound (for the fictitious Hamiltonian used here), one can use conventional quantum chemistry methods to treat it. One can then extrapolate the plot of the energy of the stabilized π^*-attached state back to $\delta q = 0$, making sure to use data only for $\delta q > 1.75$, to estimate the actual energy of the metastable state.

I should point out that if one were to stabilize by adding excess charges δq only to the two carbon nuclei, as has been done in most such applications dating back to ref 72, one can also isolate the π^* orbital from the PC orbitals. However, this approach can cause some of the PC orbitals to evolve into bound Rydberg-like orbitals (see Figure 4 in ref 65). This happens because the modified Hamiltonian's total potential now has a net positive charge.

This same δq stabilization strategy can also be used[65] for correlated methods as illustrated in Figure 25.

https://doi.org/10.1021/acs.jpca.3c01564
J. Phys. Chem. A XXXX, XXX, XXX−XXX

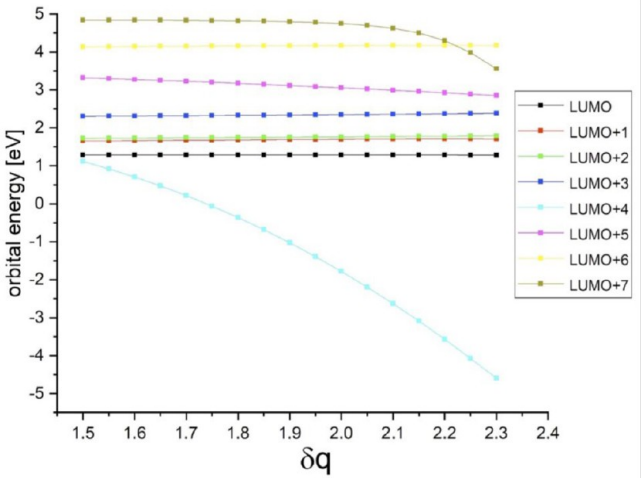

Figure 24. Energies of ethylene's virtual orbitals as a function of added partial charge; see text for detail. Reprinted with permission from Figure 10 in ref 65. Copyright 2022 American Chemical Society.

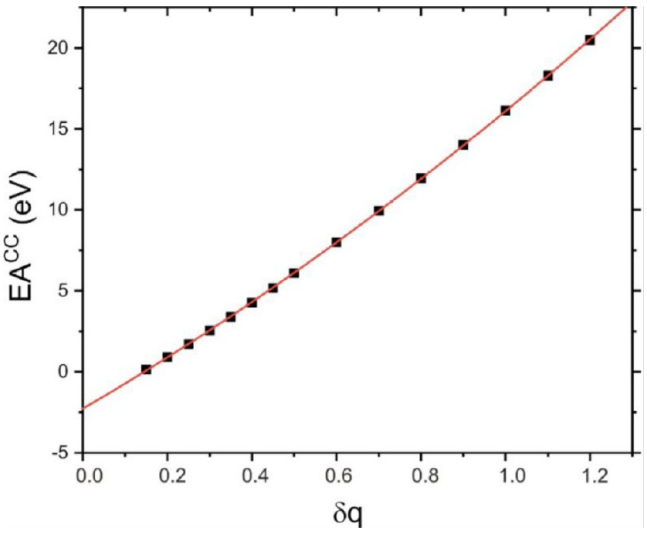

Figure 25. Ethylene EA computed at the CC level for various stabilizing partial charges. Reprinted with permission from Figure 6 in ref 65. Copyright 2022 American Chemical Society.

This plot shows the energy difference between two coupled-cluster results—one on neutral ethylene with the nuclear charges on the two C nuclei altered by δq and the other on the ethylene anion also with the modified nuclear charges, using only δq values for which the π^*-attached anion is stable. In this case, the extrapolation predicts[65] an energy of ca. 2.3 eV (electron transmission experiments suggest a value near 1.8 eV).

This is not the only way to differentially stabilize a valence-type metastable state relative to PC states. Other approaches[73,74] involve adding different external potentials (e.g., stabilizing positive partial charges surrounding the anion's periphery or adding a "box" potential to differentially stabilize valence-range orbitals relative to PC orbitals) to effect the differential stabilization, but they are all aimed at the same goal.

A different type of stabilization method[75] is employed to determine both the energy and lifetime of a metastable state. In a commonly used approach,[69,70,76] one scales the orbital exponents of the more diffuse basis functions by an amount α ($\alpha < 1.0$ makes the orbitals more diffuse; $\alpha > 1$ makes them more spatially compact). One then computes the energies of several electron-attached states (e.g., using *KT* at the most basic level or coupled-cluster anion-neutral energy differences or EOM-EA-CCSD at higher levels) and plots the energies of these states relative to that of the neutral as a function of α. An example of such a so-called stabilization plot for the uracil anion obtained by Spiridoula Matsika's group[76] is shown in Figure 26 where the data are the solutions at the EOM-EA-CC level.

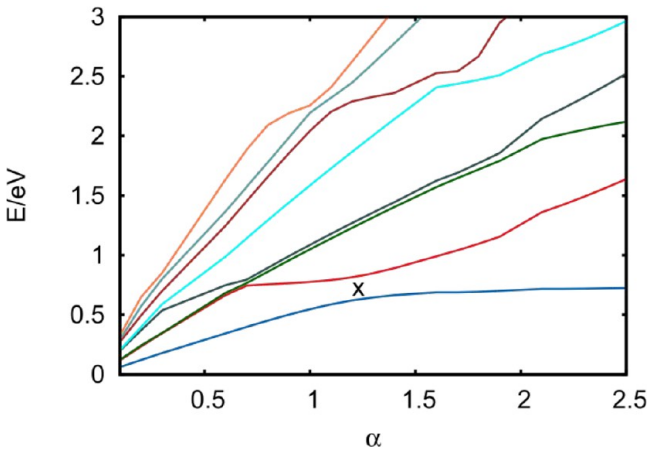

Figure 26. Stabilization plot for uracil anion. Adapted with permission from Figure 8 in ref 76. Copyright 2019 AIP Publishing.

The key ingredients in such a plot are the two curves shown in red and blue that appear to undergo an avoided crossing near $\alpha = 1.25$. The blue curve to the right of $\alpha = 1.25$ seems to be rather stable (i.e., to have a small α-dependence) while the red curve monotonically and more steeply increases with $\alpha > 1.25$.

The most elementary route making use of such a stabilization graph is to view the avoided crossing to arise from the coupling of a valence-range metastable state (i.e., the blue curve) whose energy as a function of α is denoted $H_{1,1}$ and a PC state (i.e., the red curve) with energy $H_{2,2}$ coupled by an amount V, one can imagine solving for the eigenvalues of the resulting 2×2 Hamiltonian matrix. The quadratic equation resulting from this approach

$$E^2 - E(H_{1,1} + H_{2,2}) + H_{1,1}H_{2,2} - V^2 = 0 \tag{5}$$

yields two solutions

$$E_{\pm} = (H_{1,1} + H_{2,2})/2 \pm 1/2\sqrt{V^2 + (H_{2,2} - H_{1,1})^2} \tag{6}$$

In its most elementary version, the α-dependences of $H_{1,1}$ and of $H_{2,2}$ are assumed to be linear, and the coupling V is assumed to be constant. Using these "fits" in the expression for $E_{\pm}$ and then setting to zero the derivative of $E_{\pm}$ with respect to α (to find a stable point), gives an expression[77] for the stable α which, when substituted into $E_{\pm}$ gives

$$E = E_C - 2iV\frac{\sqrt{s_V s_{PC}}}{s_{PC} - s_V} \tag{7}$$

Here s_V is the slope of the blue valence-type curve and s_{PC} is the slope of the red PC curve, and E_C is the energy at which the linear fits to $H_{1,1}$ and of $H_{2,2}$ intersect. The imaginary part of this energy is the half-width $\Gamma/2$ of the metastable state whose lifetime τ is given by $\tau = 2\hbar/\Gamma$.

https://doi.org/10.1021/acs.jpca.3c01564
J. Phys. Chem. A XXXX, XXX, XXX−XXX

A more sophisticated and widely used approach,[70] still using stabilization graph data as in Figure 26, involves expressing the eigenvalue solution equation as

$$R(\alpha)E^2 - P(\alpha)E + Q(\alpha) = 0 \tag{8}$$

with R, P, and Q expressed as polynomials in α (effectively allowing $H_{1,1}$, $H_{2,2}$, and V to be more flexible functions of α). One then uses energy data from the red and blue curves at a range of α values in eq 8 to determine the coefficients in the R, P, and Q polynomials. Then, one sets $\frac{dE}{d\alpha} = 0$ with

$$E = 1/2\left[\frac{P(\alpha)}{R(\alpha)} \pm \frac{1}{R(\alpha)}\sqrt{P(\alpha)^2 - 4Q(\alpha)R(\alpha)}\right] \tag{9}$$

to identify the critical value of α. Inserting this α value back into eq 9 then give the complex value of E. The real part of E is the energy of the metastable state and the imaginary part is the half-width $\Gamma/2$. In the paper[76] cited from the Matsika group and in another of their work,[71] the method of ref 70 was applied to several metastable anions and compared to results obtained using other approaches[76] including CAP.

Another approach[78−80] has been developed for determining lifetimes from the type of charge stabilization data illustrated in Figure 25. This involves creating an expression for how the energy $E(Z)$ of the artificially stabilized state depends on the parameter Z governing the strength of the stabilization. If this expression can describe the evolution of $E(Z)$ toward $Z \rightarrow 0$, it can be used to determine the complex value of E in the absence of the stabilizing potential. It turns out this requires $E(Z)$ to have terms varying as $\sqrt{Z - Z_0}$ where Z_0 is the value of Z at which E changes sign passing into the region where the state is metastable. One problem with this approach involves how the charge-stabilization can cause some of the PC states to become stabilized (i.e., to develop Rydberg character) to an extent that the $E(Z)$ data computed for the stabilized valence state of interest can not be followed all the way to Z_0, thus limiting the reliability of the $Z \rightarrow 0$ extrapolation. An example of this issue is shown in Figure 6 of ref 69. Nevertheless, this approach is showing much promise and I believe is likely to become more widely used by chemists in the near future.

In the CAP approach,[66−68,71,72] one adds to the electronic Hamiltonian H an imaginary[81] one-electron operator $-i\eta W$ whose strength is adjusted through a scale parameter η. A commonly used so-called box form for W is expressed as

$$W(x, y, z) = W_x + W_y + W_z$$

$$W_k = \begin{pmatrix} 0 & \text{if } |r_k| \le R_k \\ (r_k - R_k)^2 & \text{if } |r_k| > R_k \end{pmatrix} \tag{10}$$

where r_k are the Cartesian coordinates of the electron and the R_k parameters define the onset of the potential along the three directions. A one-dimensional example appears in Figure 27 with W shown as the thick black line. The electronic potential in the absence of W is depicted by the thin black line illustrating, for example, a valence-range attractive well and centrifugal or RCB barriers.

The idea behind this tool is for W to have little to no effect within a region "inside" the box thus allowing a valence-type resonance function (the red curve) to be unaltered while allowing W to strongly affect the energies of the PC functions (the dashed curves) whose amplitudes extend outside the valence region. Thomas Sommerfeld has introduced a so-called Voronoi potential[83] that surrounds the molecule more smoothly as illustrated in Figure 28. He has also produced a nice overview[84] of how CAP, stabilization, and other methods work by showing results for a model potential.

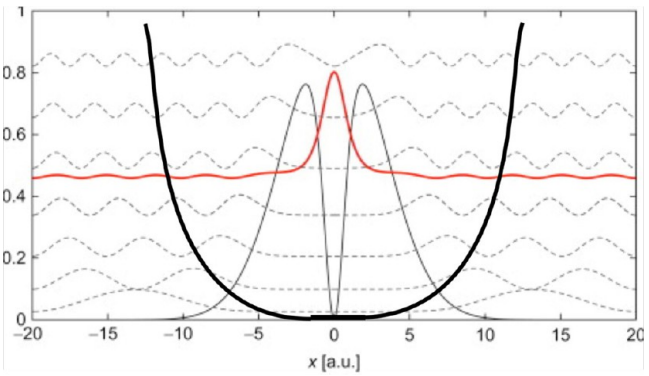

Figure 27. Illustration of a flat-bottomed box potential used in CAP calculations. Adapted with permission from Figure 1.8 of ref 82. Copyright 2012 Elsevier.

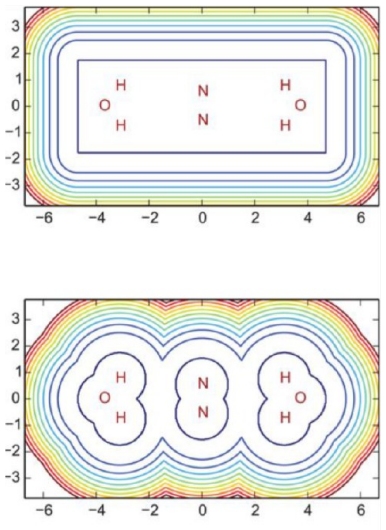

Figure 28. Illustration of flat-bottom box (top) and Voronoi (bottom) potentials used in CAP calculation on N_2 $(H_2O)_2$. Reprinted with permission from Figure 1 in ref 83. Copyright 2015 American Chemical Society.

In a CAP calculation, one carries out a quantum chemistry calculation using $H - i\eta W$ as the Hamiltonian, which results in complex energies E_K that will depend of the parameter η and on the location of the box origin and its range. If the box parameters are chosen appropriately (to have little effect on the metastable function while strongly altering the PC functions), one can find a complex eigenvalue whose dependence on the η parameter can be made stable ($\frac{dE}{d\eta} = 0$); at this value of η, the real part of the energy E is the metastable state's energy and the imaginary part is its half-width.

The search for the value of η that meets the stability criterion is usually carried out by performing calculations using a series of η values and then plotting the complex energies obtained at these η values. An example is shown in Figure 29 from Matsika's group's work on the p-benzoquinone anion.[76]

https://doi.org/10.1021/acs.jpca.3c01564
J. Phys. Chem. A XXXX, XXX, XXX−XXX

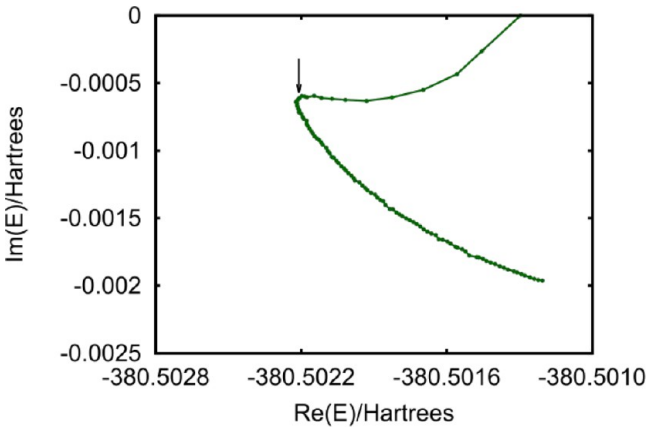

Figure 29. Plot of real and imaginary values of the complex energy resulting in a CAP calculation on p-benzoquinone anion. The point of stability is denoted with an arrow. Adapted with permission from Figure 7 in ref 76. Copyright 2019 AIP Publishing.

The green curve consists of a series of points at various values of η. The point at which the stability condition $\frac{dE}{d\eta} = 0$ is reached is labeled with an arrow. Notice that this condition means both the real and imaginary parts of E are supposed to have zero derivatives at this point.

In Figure 30, I show a conventional stabilization graph also for p-benzoquinone from Matsika's work[76] in which an avoided crossing appears near 0.8 eV.

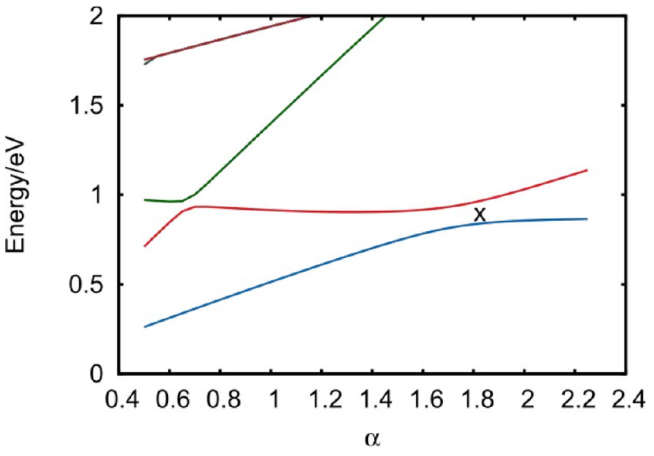

Figure 30. Stabilization plot for p-benzoquinone anion. Adapted with permission from Figure 6 in ref 76. Copyright 2019 AIP Publishing.

In that work, fitting data from the stabilization graph to the functional form in eq 9 using R, P, and Q polynomials of third order in α, the workers obtained an energy of 0.86 eV and a width of 0.008 eV. In comparison, when employing the CAP method as in Figure 29, these same workers found an energy of 0.99 eV and a width of 0.033 eV. They report an experimental values of 1.35 and 0.025 eV, respectively.

Recently, Ksenia Bravaya's group reported results[85] using CAP at the EOM-CCSD level applied to a large number of metastable MAs including anions of N_2, CO, HCN, CO_2, H_2CO, C_2H_4, uracil, naphthalene (and derivatives), chloroethylene, and *p*-benzoquinone. In that work and another[86] in which she used a Voronoi variant of the box potential to study N_2 $(H_2O)_2$ and $(CO_2)_2$ clusters, one can see excellent evidence of how the CAP method is employed successfully.

Before ending this discussion of metastable MAs, I want to explain how such species can be rendered stable not by artificial partial positive charges as in the Nestmann−Peyerimhoff approach I explained earlier but by actual positive charges within the molecule. In electron capture dissociation (ECD) mass spectrometry, when a gaseous sample of a polypeptide is exposed to low-energy free electrons, a very specific type of bond cleavage is observed: cleavage of N-C_α bonds. We proposed[87] that this cleavage occurs when an electron is captured into a π^* orbital of the O═C−N unit as shown in Figure 31.

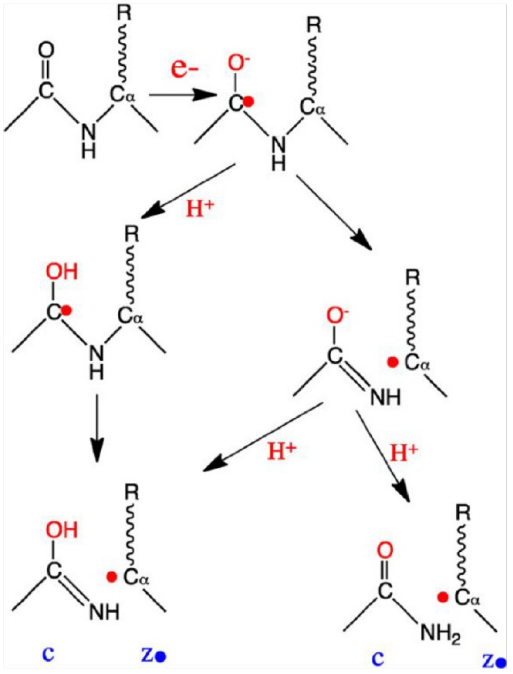

Figure 31. Mechanism of N-C_α bond cleavage by electron capture. Reprinted with permission from Scheme 1 in ref 87. Copyright 2014 American Chemical Society.

However, capture into such an orbital is known[87] to produce a metastable π^*-attached state lying ca. 2 eV above the energy of the corresponding neutral. It turns out that the Coulomb potentials of the positively charged groups (often protonated side chains) $\sum_{protonated\ sites\ a} \frac{14.4}{R_a}$ within the polypeptide can produce stabilization sufficient to render the π^*-attached state stable if their distances R_a to the O═C−N unit are sufficiently small.

4. DISCUSSION AND CONCLUSIONS

I hope this adventure through the world of MAs has shown why these species are interesting, important to chemistry, and challenging to study theoretically or experimentally. In recent decades, many new-generation workers have entered the field, and I have tried to highlight several of them here (sorry, length limitations on Perspectives precluded recognizing more). Several very diverse families of MAs have been shown to exist. Some hold their excess electron loosely (e.g., dipole, quadrupole, polarization-bound) and occur in space, at interfaces, and as potential doorways to bond breaking. Others bind their electrons even more tightly than do halogen anions. Multiply

https://doi.org/10.1021/acs.jpca.3c01564
J. Phys. Chem. A XXXX, XXX, XXX−XXX

charged MAs possess internal Coulomb potentials that alter intrinsic electron binding strengths and produce RCBs that can result in metastability. In molecules containing positively charged groups, Coulomb potentials can render metastable MA states stable. So, the EBEs of MAs can differ from one environment to another (e.g., when stabilized by counter cations, at air−water or air-ice interfaces vs when fully solvated, with nearby positively charged groups that stabilize or negative groups that destabilize).

AUTHOR INFORMATION

Corresponding Author

Jack Simons − *Henry Eyring Center for Theoretical Chemistry, Department of Chemistry, University of Utah, Salt Lake City, Utah 84112, United States;* orcid.org/0000-0001-8722-184X; Email: jack.simons@utah.edu

Complete contact information is available at: https://pubs.acs.org/10.1021/acs.jpca.3c01564

Notes

The author declares no competing financial interest.

Biography

Jack Simons earned his Ph.D. under Prof. John Harriman at the University of Wisconsin in 1970. After postdoctoral study under Prof. John Deutch at MIT, he joined the University of Utah faculty in 1971 where he rose through the ranks eventually holding the Henry Eyring Chair. He became Emeritus in 2011, but remains active in research and service. He created a web page on Theoretical Chemistry (https://simons.hec.utah.edu/TheoryPage/index.html) and a series of YouTube videos on electronic structure theory (https://simons.hec.utah.edu/YouTubeLinks.html). In 2008, he founded the Telluride Schools on Theoretical Chemistry (https://telluridescience.org/schools/theoretical-chemistry/), and in 2022 the ACS PHYS Division named their senior Award in Theoretical Chemistry after him.

ACKNOWLEDGMENTS

The author thanks the reviewers for constructive feedback. There is no financial support to acknowledge.

REFERENCES

(1) Simons, J. Molecular Anions. *J. Phys. Chem. A* **2008**, *112*, 6401−6511.

(2) Jordan, K. D.; Voora, V. K.; Simons, J. Negative electron affinities from conventional electronic structure methods. *Theor. Chem. Acc.* **2014**, *133*, 1445.

(3) A good source compiling atomic and molecular electron affinities determined by experiment and theory is Rienstra-Kiracofe, J. C.; Tschumper, G. S.; Schaefer, H. F.; Nandi, S.; Ellison, G. B. Atomic and Molecular Electron Affinities: Photoelectron experiments and Theoretical Computations. *Chem. Rev.* **2002**, *102*, 231−282.

(4) Lecomte, F.; Schermann, J. P.; Desfrancois, C. In *Theoretical Prospect of Negative Ions*, Kalcher, J., Ed.; Research Signpost: 2002; pp 29−41.

(5) This article provides a good survey especially as related to chemistry Jordan, K. D.; Wang, F. Theory of Dipole-Bound Anions. *Annu. Rev. Phys. Chem.* **2003**, *54*, 367−396.

(6) An excellent overview of such loosely bound electrons is provided in Herbert, J. M. In *Reviews of Computational Chemistry*, Parrill, A. L., Lipkowitz, K. B.; Eds., 2015; Vol. *28*; pp 391−517.

(7) Simons, J. Ejecting Electrons from Molecular Anions via Shine, Shake/Rattle, and Roll. *J. Phys. Chem. A* **2020**, *124*, 8778−8797.

(8) Simons, J. Propensity Rules for Vibration-Induced Electron Detachment of Anions. *J. Am. Chem. Soc.* **1981**, *103*, 3971−3976.

(9) A nice recent study of the ethylene anion is given in Sommerfeld, T.; Melugin, J. B.; Ehara, M. Temporary Anion States of Ethene Interacting with Single Molecules of Methane, Ethane, and Water. *J. Phys. Chem. A* **2018**, *122*, 2580−2586.

(10) Dreuw, A.; Cederbaum, L. S. In *Theoretical Prospect of Negative Ions*, Kalcher, J., Ed.; Research Signpost: 2002; pp 1−28.

(11) Dreuw, A.; Cederbaum, L. S. Nature of the Repulsive Coulomb barrier in multiply charged negative ions. *Phys. Rev. A* **2000**, *63*, 012501.

(12) Boldyrev, A. I.; Simons, J. Is TeF_8^{2-} the MX_n^{2-} Dianion with the Largest Electron Detachment Energy (5 eV)? *J. Chem. Phys.* **1992**, *97*, 2826−2827.

(13) Wang, X.-B.; Wang, L.-S. Photoelectron Spectroscopy of Multiply Charged Anions. *Annu. Rev. Phys. Chem.* **2009**, *60*, 105−126.

(14) Wang, X.-B.; Ding, C.-F.; Nicholas, J. B.; Dixon, D. A.; Wang, L.-S. Investigation of Free Singly and Doubly Charged Alkali Metal Sulfate Ion Pairs: $M^+(SO_4^{2-})$ and $[M^+(SO_4^{2-})]_2$ (M = Na, K). *J. Phys. Chem. A* **1999**, *103*, 3423−3429.

(15) Simons, J.; Skurski, P. In *Theoretical Prospect of Negative Ions*, Kalcher, J., Ed.; Research Signpost, 2002; pp 117−138.

(16) Gibbard, J. A.; Verlet, J. R. R. Kasha's Rule and Koopmans' Correlations for Electron Tunneling through Repulsive Coulomb Barriers in a Polyanion. *J. Phys. Chem. Lett.* **2022**, *13*, 7797−7801.

(17) Horke, D. A.; Chatterley, A. S.; Verlet, J. R. R. Effect of Internal Energy on the Repulsive Coulomb Barrier of Polyanions. *Phys. Rev. Lett.* **2012**, *108*, 083003.

(18) Jarrold, C. C. Probing Anion-Molecule Complexes of Atmospheric Relevance Using Anion Photoelectron Detachment Spectroscopy. *ACS Phys. Chem. Au* **2023**, *3*, 17−29.

(19) Mason, J. L.; Folluo, C. N.; Jarrold, C. C. More than little fragments of matter: Electronic and molecular structures of clusters. *J. Chem. Phys.* **2021**, *154*, 200901.

(20) Aikens, C. M.; Jarrold, C. C. Virtual Issue of Experiment-Theory Synergies in the Study of Metal and Metal-Containing Clusters. *J. Phys. Chem. A* **2023**, *127*, 3−5. This issue of the journal offers many examples of related work.

(21) Liu, G.; Poths, P.; Zhang, X.; Zhu, Z.; Marshall, M.; Blankenhorn, M.; Alexandrova, A. N.; Bowen, K. H. CO_2 Hydrogenation to Formate and Formic Acid by Bimetallic Palladium-Copper Hydride Clusters. *J. Am. Chem. Soc.* **2020**, *142*, 7930−7936.

(22) Wong, N. G. K.; Rankine, C. D.; Anstöter, C. S.; Dessent, C. E. H. Photostability of the deprotonated forms of the UV filters homosalate and octyl salicylate: molecular dissociation versus electron detachment following UV excitation. *Phys. Chem. Chem. Phys.* **2022**, *24*, 17068−17076.

(23) Gutsev, G. L.; Boldyrev, A. I. DMV-Xα calculations on the ionization potentials of MX_{k+1}^- complex anions and the electron affinities of MX_{k+1} "superhalogens. *Chem. Phys.* **1981**, *56*, 277−283.

(24) An excellent review is provided in Skurski, P. In *Superatoms: Principles, Synthesis, and Applications*; Jena, P.; Sun, Q., Eds., John Wiley and Sons, Ltd.: 2021; Chapter 3.

(25) Cyraniak, A.; Faron, D.; Freza, S.; Anusiewicz, I.; Skurski, P. . Superhalogen anions supported by the systems comprising alternately aligned boron and nitrogen central atoms. *Front. Chem.* **2022**, *10*, 863408.

https://doi.org/10.1021/acs.jpca.3c01564
J. Phys. Chem. A XXXX, XXX, XXX−XXX

(26) Ariyarathna, I. R.; Khan, S. N.; Pawlowski, F.; Ortiz, J. V.; Miliordos, E. Aufbau Rules for Solvated Electron Precursors: $Be(NH_3)_4^{0,\pm}$ Complexes and Beyond. *J. Phys. Chem. Lett.* **2018**, *9*, 84−88.
(27) Ariyarathna, I. R.; Pawlowski, F.; Ortiz, J. V.; Miliordos, E. Aufbau Principle for Diffuse Electrons of Double-Shell Metal Ammonia Complexes: The Case of $M(NH_3)_4$@$12NH_3$, M = Li, Be^+, B^{2+}. *J. Phys. Chem. A* **2020**, *124*, 505−512.
(28) Hopper, H.; Lococo, M.; Dolgounitcheva, O.; Zakrzewski, V. G.; Ortiz, J. V. Double-Rydberg Anions: Predictions on $NH_3AH_n^-$ and $OH_2AH_n^-$ Structures. *J. Am. Chem. Soc.* **2000**, *122*, 12813−12818.
(29) Ortiz, J. V. Vertical and adiabatic ionization energies of NH_4^- isomers via electron propagator theory and many body perturbation theory calculations with large basis sets. *J. Chem. Phys.* **1987**, *87*, 3557−3562.
(30) Bowen, K. H.; Eaton, J. G. In *The Structure of Small Molecules and Ions*; Naaman, R.; Vager, Z., Eds.; Plenum Press: 1987; p 147.
(31) Mucha, M.; Frigato, T.; Levering, L. M.; Allen, H. C.; Tobias, D. J.; Dang, L. X.; Jungwirth, P. Unified Molecular Picture of the Surfaces of Aqueous Acid, Base, and Salt Solutions. *J. Phys, Chem. B* **2005**, *109*, 7617−7623.
(32) Lee, J. K.; Walker, K. L.; Han, H. S.; Kang, J.; Prinz, F. B.; Waymouth, R. M.; Nam, H. G.; Zare, R. N. Spontaneous generation of hydrogen peroxide from aqueous microdroplets. *Proc. Natl. Acad. Sci. U. S. A.* **2019**, *116*, 19294−19298.
(33) Kathmann, S. M.; Kuo, I. F. W.; Mundy, C. J. Electronic effects on the surface potential at the vapor−liquid interface of water. *J. Am. Chem. Soc.* **2008**, *130*, 16556−16561.
(34) Buch, V.; Milet, A.; Vacha, R.; Jungwirth, P.; Devlin, J. P. Water surface is acidic. *Proc. Natl. Acad. Sci. U. S. A.* **2007**, *104*, 7342−7347.
(35) Chen, H.; Wang, R.; Xu, J.; Yuan, X.; Zhang, D.; Zhu, D.; Marshall, M.; Bowen, K. H.; Zhang, X. Spontaneous Reduction by One Electron on Water Microdroplets Facilitates Direct Carboxylation with CO_2. *J. Am. Chem. Soc.* **2023**, *145*, 2647−2652.
(36) Roscioli, J. R.; Hammer, N. I.; Johnson, M. A.; Diri, K.; Jordan, K. D. Exploring the correlation between network structure and electron binding energy in the $(H_2O)_7^-$ cluster through isomer-photoselected vibrational predissociation spectroscopy and ab initio calculations: Addressing complexity beyond types I-III. *J. Chem. Phys.* **2008**, *128*, 104314.
(37) See, for example Liu, G.; Ciborowski, S.; Graham, J.; Buytendyk, A.; Bowen, K. Photoelectron Spectroscopic Study of Dipole-bound and Valence-bound Nitromethane Anions Formed by Rydberg Electron Transfer. *J. Chem. Phys.* **2020**, *153*, 044307.
(38) For example Skurski, P.; Gutowski, M.; Simons, J. How to Choose a One-Electron Basis Set to Reliably Describe a Dipole-Bound Anion. *Int. J. Quantum Chem.* **2000**, *80*, 1024−1038.
(39) Gutowski, M.; Skurski, P.; Boldyrev, A. I.; Simons, J.; Jordan, K. The Contribution of Electron Correlation to the Stability of Dipole-Bound Anionic States. *Phys. Rev.* **1996**, *54*, 1906−1909.
(40) Fortenberry, R. C. Interstellar Anions: The Role of Quantum Chemistry. *J. Phys. Chem. A* **2015**, *119*, 9941−9953.
(41) Millar, T. J.; Walsh, C.; Field, T. A. Negative Ions in Space. *Chem. Rev.* **2017**, *117*, 1765−1795.
(42) Young, R. M.; Neumark, D. M. Dynamics of Solvated Electrons in Clusters. *Chem. Rev.* **2012**, *112*, 5553−5577.
(43) Bradforth, S. E.; Jungwirth, P. Excited States of Iodide Anions in Water: A Comprison of the Electronic Structures in Clusters and in Bulk Solution. *J. Phys. Chem. A* **2002**, *106*, 1286−1298.
(44) This is also discussed in ref 6.
(45) Burrow, P. D.; Gallup, G. A.; Scheer, A. M.; Denifl, S.; Ptasinska, S.; Märk, T.; Scheier, T. Vibrational Feshbach resonances in uracil and thymine. *J. Chem. Phys.* **2006**, *124*, 124310.
(46) Kang, D. H.; Kim, J.; Eun, H. J.; Kim, S. K. Experimental Observation of the Resonant Doorways to Anion Chemistry: Dynamic Role of Dipole-Bound Feshbach Resonances in Dissociative Electron Attachment. *J. Am. Chem. Soc.* **2022**, *144*, 16077−16085.
(47) Anusiewicz, I.; Skurski, P.; Simons, J. Fate of Dipole-Bound Anion States when Hydrated. *J. Phys. Chem. A* **2020**, *124*, 2064−2076.
(48) Simons, J. How Do Low-Energy (0.1−2 eV) Electrons Cause DNA Strand Breaks? *Acc. Chem. Res.* **2006**, *39*, 772−779.
(49) Martin, F.; Burrow, P. D.; Cai, Z.; Cloutier, P.; Hunting, D.; Sanche, L. DNA Strand Breaks Induced by 0−4 eV Electrons: The Role of Shape Resonances. *Phys. Rev. Lett.* **2004**, *93*, 068101.
(50) Zheng, Y.; Cloutier, P.; Hunting, D.; Sanche, L.; Wagner, J. R. Chemical Basis of DNA Sugar-Phosphate Cleavage by Low- Energy Electrons. *J. Am. Chem. Soc.* **2005**, *127*, 16592−16598.
(51) Cooper, G. A.; Clarke, C. J.; Verlet, J. R. R. Low-Energy Shape Resonances of a Nucleobase in Water. *J. Am. Chem. Soc.* **2023**, *145*, 1319−1326.
(52) Rogers, J. P.; Anstöter, C. S.; Verlet, J. R. R. Ultrafast dynamics of low-energy electron attachment via a non-valence correlation-bound state. *Nat. Chem.* **2018**, *10*, 341−346.
(53) Rogers, J. P.; Anstöter, C. S.; Bull, J. N.; Curchod, B. F. R.; Verlet, J. R. R. Photoelectron Spectroscopy of the Hexafluorobenzene Cluster Anions: $(C_6F_6)_n^-$ (n = 1−5) and $I^-(C_6F_6)$. *J. Phys. Chem. A* **2019**, *123*, 1602−1612.
(54) Verlet, J. R. R.; Anstöter, C. S.; Bull, J. N.; Rogers, J. P. Role of Nonvalence States in the Ultrafast Dynamics of Isolated Anions. *J. Phys. Chem. A* **2020**, *124*, 3507−3519.
(55) Voora, V. K.; Jordan, K. D. Non-valence Correlation Bound Anion State of C_6F_6: Doorway to Low-Energy Electron Capture. *J. Phys. Chem. A* **2014**, *118*, 7201−7205.
(56) Hart, A. C.; Lyle, J.; Spellberg, J.; Krylov, A. I.; Mabbs, R. Role of the Electron-Dipole Interaction in Photodetachment Angular Distributions. *J. Phys. Chem. Lett.* **2021**, *12*, 10086−10092.
(57) Sanov, A. Laboratory-Frame Photoelectron Angular Distributions in Anion Photodetachment: Insight into Electronic Structure and Intermolecular Interactions. *Annu. Rev. Phys. Chem.* **2014**, *65*, 341−363.
(58) Grumbling, E. R.; Sanov, A. Photoelectron Angular Distributions in Negative-Ion Photodetachment from Mixed sp States. *J. Chem. Phys.* **2011**, *135*, 164302.
(59) Ortiz, J. V. Toward an exact one electron picture of chemical bonding. *Adv. Quantum Chem.* **1999**, *35*, 33−52.
(60) A person very influential in bringing Dyson orbitals into modern quantum chemistry is Vince Ortiz. See ref 59 and Ortiz, J. V. Dyson-orbital concepts for description of electrons in molecules. *J. Chem. Phys.* **2020**, *153*, 070902.
(61) Oana, C. M.; Krylov, A. I. Cross sections and photoelectron angular distributions in photodetachment from negative ions using equations-of-motion couple-cluster Dyson orbitals. *J. Chem. Phys.* **2009**, *131*, 124114.
(62) Jagau, T.-C.; Dao, D. B.; Holtgrewe, N. S.; Krylov, A. I.; Mabbs, R. Same but Different: Dipole-Stabilized Shape Resonances in CuF^- and AgF^-. *J. Phys. Chem. Lett.* **2015**, *6*, 2786−2793.
(63) Jagau, T.-C. Theory of electronic resonances: fundamental aspects and recent advances. *Chem. Commun.* **2022**, *58*, 5205−5224.
(64) Jagau, T.-C.; Bravaya, K. B.; Krylov, A. I. Extending Quantum Chemistry of Bound States to Electronic Resonances. *Annu. Rev. Phys. Chem.* **2017**, *68*, 525−553.
(65) Anusiewicz, I.; Skurski, P.; Simons, J. Finding Valence Antibonding Levels while Avoiding Rydberg, Pseudo-continuum, and Dipole-Bound Orbitals. *J. Am. Chem. Soc.* **2022**, *144*, 11348−11363.
(66) Riss, U. V.; Meyer, H.-D. Calculation of Resonance Energies and Widths using the Complex Absorbing Potential Method. *J. Phys. B: At., Mol. Opt. Phys.* **1993**, *26*, 4503−4535.
(67) Sommerfeld, T.; Riss, U. V.; Meyer, H.-D.; Cederbaum, L. S.; Engels, B.; Suter, H. U. Temporary Anions - Calculation of Energy and Lifetime by Absorbing Potentials: The N_2^- $^2\Pi_g$Resonance. *J. Phys. B: At., Mol.Opt.Phys.* **1998**, *31*, 4107−4122.
(68) Santra, R.; Cederbaum, L. S. Complex absorbing potentials in the framework of electron propagator theory. I. General formalism. *J. Chem. Phys.* **2002**, *117*, 5511−5521.
(69) Much of what I overview here is treated in more detail in Simons, J. Analysis of Stabilization and Extrapolation Methods for Determining Energies and Lifetimes of Metastable Electronic States. *J. Phys. Chem. A* **2021**, *125*, 7735−7749.

https://doi.org/10.1021/acs.jpca.3c01564
J. Phys. Chem. A XXXX, XXX, XXX−XXX

(70) Chao, J. S.-Y.; Falcetta, M. F.; Jordan, K. D. Application of the Stabilization Method to the $N_2^-(X^2\Pi_g)$ and $Mg^-(1^2P)$ Temporary Anion States. *J. Chem. Phys.* **1990**, *93*, 1125−1135.
(71) Fennimore, M. A.; Matsika, S. Electronic Resonances of Nucleobases Using Stabilization Methods. *J. Phys. Chem. A* **2018**, *122*, 4048−4057.
(72) Nestmann, B. M.; Peyerimhoff, S. D. CI method for determining the location and width of resonances in electron-molecule collision processes. *J. Phys. B: At. Mol. Phys.* **1985**, *18*, 4309−4319.
(73) White, A. F.; Head-Gordon, M.; McCurdy, C. W. Stabilizing potentials in bound state analytic continuation methods for electronic resonances in polyatomic molecules. *J. Chem. Phys.* **2017**, *146*, 044112.
(74) Sommerfeld, T.; Ehara, M. Short-range stabilizing potential for computing energies and lifetimes of temporary anions with extrapolation methods. *J. Chem. Phys.* **2015**, *142*, 034105.
(75) Hazi, A. U.; Taylor, H. S. Stabilization method of calculating resonance energies: Model problem. *Phys. Rev. A* **1970**, *1*, 1109−1120.
(76) Thodika, M.; Fennimore, M.; Karsili, T. N. V.; Matsika, S. Comparative study of methodologies for calculating metastable states of small to medium-sized molecules. *J. Chem. Phys.* **2019**, *151*, 244104.
(77) Simons, J. Resonance State Lifetimes from Stabilization Graphs. *J. Chem. Phys.* **1981**, *75*, 2465−2467.
(78) Horáček, J.; Mach, P.; Urban, J. Calculation of S-Matrix Poles by Means of Analytic Continuation in the Coupling Constant: Application to the $^2\Pi_g$ State of N_2^-. *Phys. Rev. A* **2010**, *82*, 032713.
(79) Papp, P.; Matejcik, Š.; Mach, P.; Urban, J.; Paidarova, I.; Horáček, J. Analytical Continuation in Coupling Constant Method; Application to the Calculation of Resonance Energies and Widths for Organic Molecules: Glycine, Alanine and Valine and Dimer of Formic Acid. *Chem. Phys.* **2013**, *418*, 8−13.
(80) Horáček, J.; Paidarová, I.; Čurík, R. On a simple way to calculate electronic resonances for polyatomic molecules. *J. Chem. Phys.* **2015**, *143*, 184102.
(81) This brings one into Moiseyev's world of non-Hermitian quantum mechanics: Moiseyev, N. *Non-Hermitian Quantum Mechanics*; Cambridge University Press: Cambridge, U.K., 2011.
(82) Klaiman, S.; Gilary, I. Chapter 1- On Resonances: A First Glance into the Behavior of Unstable States. *Adv. Quantum Chem.* **2012**, *63*, 2−31.
(83) Sommerfeld, T.; Ehara, M. Complex Absorbing Potentials with Voronoi Isosurfaces Wrapping Perfectly around Molecules. *J. Chem. Theory Comput.* **2015**, *11*, 4627−4633.
(84) Davis, J. U., Jr; Sommerfeld, T. Computing resonance energies directly: method comparison for a model potential. *Eur. Phys. J. D* **2021**, *75*, 316.
(85) Gayvert, J. R.; Bravaya, K. B. Projected CAP-EOM-CCSD method for electronic resonances. *J. Chem. Phys.* **2022**, *156*, 094108.
(86) Gayvert, J. R.; Bravaya, K. B. Application of Box and Voronoi CAPs for Metastable Electronic States in Molecular Clusters. *J. Phys. Chem. A* **2022**, *126*, 5070−5078.
(87) Anusiewicz, I.; Skurski, P.; Simons, J. Refinements to the Utah-Washington Mechanism of Electron Capture Dissociation. *J. Phys. Chem. B* **2014**, *118*, 7892−7901.

https://doi.org/10.1021/acs.jpca.3c01564
J. Phys. Chem. A XXXX, XXX, XXX−XXX